JOURNAL OF GEOPHYSICAL RESEARCH, VOL. 102, NO. A5, PAGES 9513–9530, MAY 1, 1997

Equilibrium conditions for the tangential discontinuity magnetopause

J. De Keyser and M. Roth

Belgian Institute for Space Aeronomy, Brussels

Abstract. Early satellite observations of the dayside magnetopause have suggested that the magnetic field typically rotates clockwise above the solar-magnetospheric equatorial plane and counterclockwise below it, in agreement with the predictions of first-order orbit theory for magnetopause crossings of the rotational discontinuity type. The present paper treats the tangential discontinuity (TD) case. The influence of magnetosheath magnetic field and plasma flow on the magnetopause equilibrium structure is analyzed by means of a Vlasov model. The nature of the current layer plays a major role; the analysis is carried out for ion-dominated, electron-dominated, and mixed layers. Necessary and sufficient conditions for the existence of an equilibrium magnetopause are derived. It is found that (1) the magnetopause is best modeled as a transition layer of mixed type; (2) for high magnetic shear the magnetic field at the dayside magnetopause preferentially rotates clockwise above the equatorial plane and counterclockwise below it, while it rotates counterclockwise above and clockwise below the equatorial plane at the tail flanks; this effect becomes more manifest as the magnetosheath flow is faster and as the difference in proton and electron transition lengths is more pronounced; (3) for low magnetic shear, TD equilibrium is expected to be lost more easily at the dawnside than at the duskside; and (4) the model provides a magnetopause thickness estimate; in particular, the low magnetic shear dawn magnetopause is predicted to be thinner than the dusk magnetopause.

Introduction

The magnetopause is the current layer associated with the transition of magnetosheath to magnetospheric magnetic field. In situ magnetic field observations confirm that locally, the magnetopause may be in a tangential discontinuity (TD) as well as a rotational discontinuity (RD) state [e.g., *Sonnerup and Cahill*, 1967]. A magnetospheric boundary layer adjacent to the inner edge of the magnetopause is often observed [e.g., *Eastman et al.*, 1976; *Phan and Paschmann*, 1996]; it is absent about 10% of the time [*Eastman et al.*, 1996]. Measurements indicate that there are instances when the magnetopause may be a TD even for very large magnetic field rotation angles [*Papamastorakis et al.*, 1984; *Paschmann et al.*, 1986; *Fuselier et al.*, 1993]. We can conclude that both the TD and the RD case may occur, regardless of whether the magnetopause is in a high or low magnetic shear configuration. The distinction between the TD and the RD magnetopause has far-reaching implications for the mass and energy transfer from the solar wind to the terrestrial magnetosphere. In this perspective it is important to assess under what conditions a TD equilibrium may exist. This is the objective of the present paper.

Historically, the first models that tried to explain the very existence of a magnetopause shielding the Earth from the harsh solar wind environment were of the TD type. Their goal was to find out under which conditions a TD magnetopause interfacing a field-free magnetosheath and a plasma-free magnetosphere could persist. Attention was paid to the flow of the magnetosheath plasma, e.g., the role of a velocity component parallel to the dipole field [*Parker*, 1967a, b, 1968, 1969; *Lerche*, 1967; *Lerche and Parker*, 1967, 1970; *Su and Sonnerup*, 1971; *Ferraro and Davies*, 1968; *Davies*, 1968, 1969]. A comprehensive discussion of the various idealizations involved in these pioneering models was given by *Willis* [1975] and *Storey and Cairo* [1979].

Sestero [1966] studied the transition between two identical plasmas moving uniformly with respect to each other in the presence of a magnetic field transverse to their relative motion. This configuration describes the low magnetic shear dawn and dusk magnetopause. The study led to some general conclusions concerning the minimum width of the transition region and the maximum change in macroscopic velocity the layer can support. Depending on the sign of the shearing flow, the transition occurs over the distance of an electron or an ion Larmor radius. The former case was called electron dominated, and the latter ion-dominated, indicating which species is characterized by a non-Maxwellian velocity distribution function (VDF) in the transition layer. The maximum velocity jump supported by an electron- or ion-dominated layer was found to be of the order of the electron or ion thermal velocity. No equilibrium is possible for larger velocity shear. Recall that the sign of the shearing flow determines the sign of the convection electric field. The orbits

Copyright 1997 by the American Geophysical Union.

Paper number 97JA00335.
0148-0227/97/97JA-00335$09.00

of ions and electrons are affected differently for both senses of the transverse motion, as there is an electric potential barrier apt to repel either protons or electrons; hence the relation between velocity shear direction and the nature of the transition.

Using a charge-neutral Parker-type model describing a field-free collimated solar wind incident on a plasma-free magnetosphere, *Wu* [1986a] found evidence for nonequilibrium conditions at the dawnside. He studied nonequilibria resulting from the insolubility of the Vlasov-Maxwell equations [*Wu*, 1986b].

To analyze the effect of relative plasma flow at the magnetopause, *Kuznetsova et al.* [1994] suggested a simple equilibrium configuration that combines the *Harris* [1962] and *Sestero* [1966] models. They considered a mixed layer (in which both ion and electron VDFs are non-Maxwellian in the transition) separating isothermal magnetosheath and magnetospheric plasmas with nearly antiparallel magnetic fields of equal strength, and with a shear flow parallel or antiparallel to the magnetic field variation across the magnetopause. The magnetic field was shown to rotate from the magnetospheric to the magnetosheath direction, rather than simply reverse its sign. For a given sense of magnetic field rotation an equilibrium was found to exist only for one particular orientation of the shear flow; for the opposite orientation no solution could be found that satisfied the boundary conditions. The model therefore indicated a relation between magnetic field behavior and magnetosheath flow direction, i.e., the magnetic field rotation sense should be opposite in the northern and southern hemispheres, as suggested by experimental data [*Sonnerup and Cahill*, 1968].

The present paper extends the work of *Kuznetsova et al.* [1994]. It addresses the existence problem of the TD equilibrium magnetopause with an advanced Vlasov model (for a recent review of such models, see *Roth et al.* [1996]) that allows an arbitrary magnetosheath flow direction. The purpose of this paper is to point out that (1) the TD magnetopause can be in equilibrium only for particular magnetosheath plasma and field conditions, (2) for high magnetic shear there is a magnetic field sense-of-rotation asymmetry between the northern and southern hemispheres, (3) TD equilibrium is expected to be lost more easily at the low magnetic shear dawn magnetopause than at the duskside, and (4) a magnetopause thickness estimate can be obtained.

The paper is organized as follows. First, the magnetopause model is presented. Then a set of necessary conditions for the existence of an equilibrium is derived. Subsequently, Maxwell's equations are used to compute the electromagnetic structure of the transition and to establish a sufficient existence condition. Numerical simulation allows us to outline the domain of relative velocities for which an equilibrium with a given magnetic field configuration can be found. Finally, a magnetopause thickness estimate is obtained. The paper concludes by discussing the implications of these theoretical results for the magnetopause, in particular regarding magnetic field rotation sense and the thickness of the current layer.

TD Magnetopause Model

The magnetopause is considered to be locally planar. This assumption is justified, as the radius of curvature of the magnetopause (several Earth radii) is much larger than its thickness (a few times the ion gyroradius [*Berchem and Russell*, 1982a]). We will adopt a reference frame (X, Y, Z) in which X is along the outward magnetopause normal and the Y, Z plane coincides with the center of the current layer. The magnetosphere corresponds to the region to the left of the magnetopause (superscript l), while the magnetosheath is situated to the right (superscript r). The Y axis is chosen along the inner bisectrix of the magnetic field vectors $\boldsymbol{B}^{\mathrm{l}}$ and $\boldsymbol{B}^{\mathrm{r}}$ (Figure 1). The plasma bulk velocities $\boldsymbol{V}^{\mathrm{l}}$ and $\boldsymbol{V}^{\mathrm{r}}$ are parallel to the layer. By means of a Galilean transformation it is always possible to obtain $\boldsymbol{V}^{\mathrm{r}} = -\boldsymbol{V}^{\mathrm{l}}$. The magnetic field variation will be denoted by $\Delta\boldsymbol{B} = \boldsymbol{B}^{\mathrm{r}} - \boldsymbol{B}^{\mathrm{l}}$, and the relative velocity between the magnetosheath and magnetospheric plasmas will be denoted by $\boldsymbol{V}_{\mathrm{r}} = \boldsymbol{V}^{\mathrm{r}} - \boldsymbol{V}^{\mathrm{l}}$. Magnetic field rotation can be quantified by the angle $\theta \in [-180°, +180°]$ between $\boldsymbol{B}^{\mathrm{l}}$ and $\boldsymbol{B}^{\mathrm{r}}$. The total angle over which the tip of the magnetic field vector rotates when tracing its variation throughout the magnetopause transition layer may differ in principle from θ by a multiple of 360°, although this occurrence is rarely observed [*Berchem and Russell*, 1982b]. In each local frame of reference comoving with either the magnetospheric or the magnetosheath plasma, the electrostatic potential $\phi(X)$ tends to a constant value far from the magnetopause. It is assumed that both constants have the same value. The arbitrary constant in the definition of $\phi(X)$ is chosen such that this value is equal to zero. The magnetic vector potential is $\boldsymbol{a} = (0, a_y(X), a_z(X))$, fixing the constants in its definition by choosing $\boldsymbol{a}(0) = \boldsymbol{0}$.

To limit the number of free parameters in the model, the magnetospheric and magnetosheath plasmas are assumed to

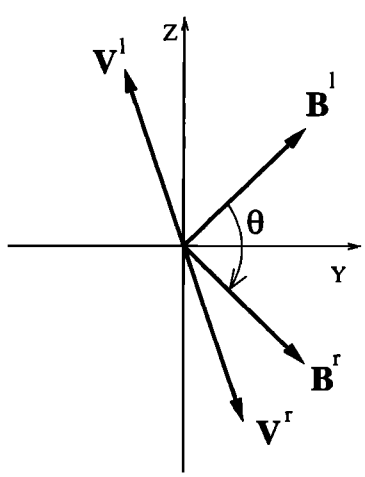

Figure 1. Projection of the magnetic field vectors $\boldsymbol{B}$ and the plasma bulk velocities $\boldsymbol{V}$ onto the locally planar TD magnetopause. Superscripts l and r identify the left (magnetospheric) and right (magnetosheath) sides, respectively. The reference frame is chosen such that $\boldsymbol{V}^{\mathrm{l}} = -\boldsymbol{V}^{\mathrm{r}}$. The Y axis is the bisectrix of the magnetic field vectors.

consist of proton and electron populations with the same temperature, although the magnetospheric plasma in reality has a higher temperature, and the protons are hotter than the electrons [*Phan and Paschmann*, 1996]. As will be discussed later, this assumption does not essentially affect our conclusions regarding the conditions for existence of an equilibrium TD, especially in the case of large velocity shear.

Different degrees of plasma and magnetic field asymmetry are known to exist at the magnetopause [e.g., *Kuznetsova and Roth*, 1995; *Eastman et al.*, 1996; *Le and Russell*, 1994; *Phan and Paschmann*, 1996]. To focus on the role of the magnetosheath flow, we will assume first that density (N^∞) and temperature (T^∞) are the same on both sides, as in earlier studies of plasma flow at the magnetopause [e.g., *Kuznetsova et al.*, 1994]; pressure balance then implies equal magnetic field magnitude ($B^\infty = B^{\mathrm{l}} = B^{\mathrm{r}}$). When a low-latitude boundary layer is present, the magnetosheath and magnetospheric plasmas may have similar density and temperature [*Phan and Paschmann*, 1996], and this hypothesis is not unrealistic. We will consider the combined effect of plasma flow and density and temperature variations at a later point in this paper.

The model makes a distinction between so-called outer and inner populations (see Figure 2). It considers four pairs of electron and proton populations: the outer left (OL) and inner left (IL) magnetospheric populations and the inner right (IR) and outer right (OR) magnetosheath populations.

Each outer (magnetospheric or magnetosheath) population has a nonzero density on one side of the transition. The fact that magnetospheric (magnetosheath) populations penetrate into the magnetosheath (magnetosphere) over only a limited distance is partly due to the existence of an electric field in the transition, but it also requires the VDFs

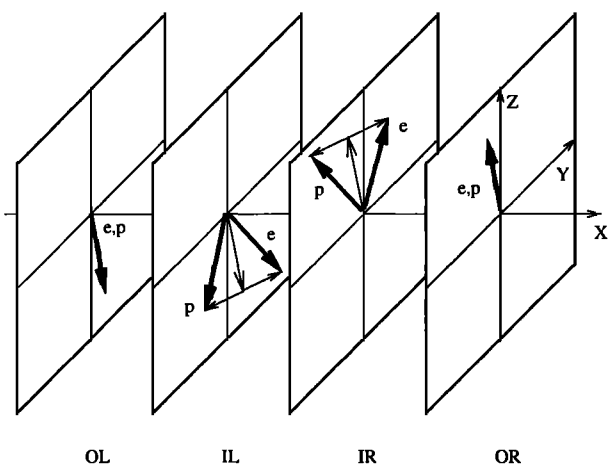

Figure 2. Mean velocities of electron (e) and proton (p) populations. The magnetospheric protons and electrons (OL+ and OL–) have the same mean velocity, which is the opposite of that of the magnetosheath particles (OR+ and OR–). The inner populations (IL+, IL–, IR+, and IR–) have an additional diamagnetic drift component; electron and proton drifts are opposite.

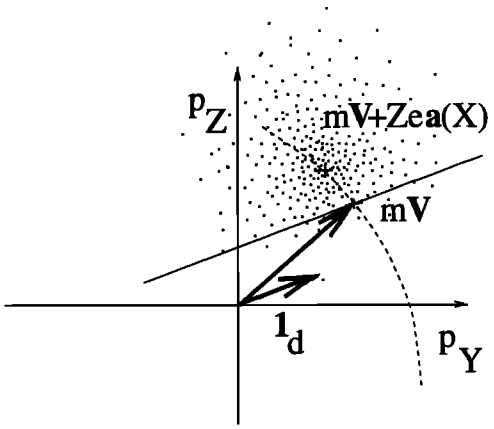

Figure 3. In this p_Y, p_Z projection of the phase space density of a population at a given position X, the effect of the cutoff in the velocity distribution function manifests itself by an abrupt decrease of the phase space density on one side of the demarcation line oriented along $\mathbf{1}_d$. As X varies, the bulk of the distribution (the point of maximum density is located at $mV + Zea(x)$) may be well above the cutoff line (purely Maxwellian distribution), near the cutoff line (anisotropic VDF), or well below it (again Maxwellian, but with its density reduced by a factor α). The abruptness of the cutoff is controlled by the characteristic length and the typical gyroradius.

of the outer proton or electron populations, or both, to be non-Maxwellian [*Sestero*, 1966]. As a particle of mass m, velocity $\boldsymbol{v}$, and charge Ze in a plane TD configuration is characterized by three constants of motion, the energy $H = \frac{1}{2}mv^2 + Ze\phi$ and the canonical momenta p_Y and p_Z ($\boldsymbol{p} = m\boldsymbol{v} + Ze\boldsymbol{a}$), this non-Maxwellian behavior can be modeled by introducing a cutoff or demarcation line in the p_Y, p_Z plane, separating magnetospheric and magnetosheath particles [e.g., *Sestero*, 1966; *Lee and Kan*, 1979; *Whipple et al.*, 1984; *Roth et al.*, 1996]. Figure 3 shows a projection of the phase space density of a particular outer population onto the p_Y,p_Z plane at a given position X. The position of the bulk of the distribution with respect to the demarcation line depends on X. When the distribution lies far from the cutoff line, it is Maxwellian, but in one half-space the population density is reduced by a prescribed factor α (possibly zero). The orientation of the demarcation line is specified by a unit vector $\mathbf{1}_d$. The abruptness of the cutoff depends on a transition length $\mathcal{L}$, typically a few times the gyroradius ρ of a thermal particle in the reference magnetic field B^∞.

An inner population (sometimes called a trapped population [*Lee and Kan*, 1979]) is associated with each outer one. Such a population has a nonzero density within the current layer only. We hypothesize that it has temperature T^∞ and that its density, n^{i}, is related to that of the corresponding outer population, n^{o}, by a given ratio $\nu = n^{\mathrm{i}}(0)/n^{\mathrm{o}}(0)$. Its mean velocity is the vector sum of the mean velocity of the corresponding outer population and an additional drift speed component. If the length scale of the diamagnetic layer is characterized by a parameter $\mathcal{L}_d$ (the physical meaning of

this parameter will become clear in the discussion of the width of the diamagnetic layer; see equation (13)), the drift speed of an inner population with temperature T is given by $V_d = 2kT/e\mathcal{L}_d B^\infty$ [*Kuznetsova et al.*, 1994]. Note that the scale length $\mathcal{L}_d$ is not arbitrary, since V_d should be at most of the order of the ion thermal velocity; it typically is a few times the ion gyroradius. Since all populations in our model are assumed to have equal temperature, proton and electron populations must have opposite drifts. These drifts $\boldsymbol{V}_d = \boldsymbol{V}_d^+ = -\boldsymbol{V}_d^-$ are oriented along the anisotropy direction ($\boldsymbol{V}_d \parallel \mathbf{1}_d$) as in the study of *Kuznetsova et al.* [1994]. They are responsible for the diamagnetic magnetopause current that shields the magnetosphere from the solar wind environment and causes the rotation of the magnetic field.

The VDF employed here is a particular version of the one discussed at length by *Roth et al.* [1996]. Analytical expressions for the moments of this VDF in terms of the electric and magnetic potentials are available. The VDF is written as a function of the constants of motion, as it then automatically satisfies the Vlasov equation of collisionless plasmas. The same form of VDF is used for outer and inner populations:

$$F = \eta(H, p_Y, p_Z) G_\alpha(u(p_Y, p_Z)),$$

with a Maxwellian at temperature T^∞ centered around a mean velocity $\boldsymbol{V}$:

$$\eta = \frac{N m^{\frac{3}{2}}}{(2\pi k T^\infty)^{\frac{3}{2}}} \exp\left(-\frac{H}{kT^\infty} - \frac{mV^2}{2kT^\infty} + \frac{p_Y V_Y + p_Z V_Z}{kT^\infty}\right),$$

and the cutoff function

$$G_\alpha = [\operatorname{erfc}(+u) + \alpha \operatorname{erfc}(-u)]/2,$$

where

$$u = ((\boldsymbol{p} - m\boldsymbol{V}) \times \mathbf{1}_d)_X / ZeB^\infty \sqrt{\mathcal{L}^2 - \rho^2},$$

$$\rho = \sqrt{2mkT^\infty}/|Z|eB^\infty = mV_{th}/|Z|eB^\infty.$$

The cutoff function is parameterized by the value of α ($0 \le \alpha \le 1$). Its argument u is proportional to the distance in the p_Y, p_Z plane between a particle's canonical momentum $\boldsymbol{p}$ and the demarcation line going through $m\boldsymbol{V}$ with direction $\mathbf{1}_d$ (see Figure 3). Note that the choice of the sign of u and the direction of the X axis implies a particular sense of $\mathbf{1}_d$. The cutoff argument also depends on the transition length $\mathcal{L}$ ($\mathcal{L} \ge \rho$). Large $\mathcal{L}$ correspond to smooth, wide transitions.

All proton and electron populations are characterized by the same transition length, $\mathcal{L}_+$ respectively $\mathcal{L}_-$, and the same density reduction factor, α_+ respectively α_-. The case $\alpha_+ = 1$ corresponds to an electron-dominated layer (as $G_1 \equiv 1$, the ion VDF remains Maxwellian), while $\alpha_- = 1$ yields an ion-dominated layer. All other situations describe mixed layers whose electromagnetic structure displays features with length scales $\mathcal{L}_+$ and $\mathcal{L}_-$. The formalism proposed here is a generalization of the one used by *Sestero* [1966] (either $\alpha_+ = 1$, $\alpha_- = 0$, $\mathcal{L}_- = \rho^-$ or $\alpha_- = 1$, $\alpha_+ = 0$, $\mathcal{L}_+ = \rho^+$, depending on the orientation of the relative velocity) and by *Kuznetsova et al.* [1994] and *De Keyser et al.* [1997] ($\alpha_\pm = 0$).

For convenience, the following dimensionless quantities are introduced:

$$\tilde{x} = x/\rho^+, \quad \tilde{\boldsymbol{B}} = \boldsymbol{B}/B^\infty, \quad \tilde{\boldsymbol{V}} = \boldsymbol{V}/V_{th}^+,$$
$$\tilde{\phi} = e\phi/kT^\infty, \quad \tilde{\boldsymbol{a}} = \boldsymbol{a}/\rho^+ B^\infty, \quad \tilde{n} = n/N^\infty,$$
$$\tilde{\boldsymbol{j}} = \boldsymbol{j}/N^\infty e V_{th}^+, \quad \lambda_\pm = \rho^+/\mathcal{L}_\pm.$$

Henceforth, dimensionless quantities will be used, and the tilde is dropped to simplify the notation. The population densities can then be written as [*Roth et al.*, 1996]

$$\begin{aligned} n^{ol\pm} &= N^{ol\pm} e^{\mp\phi \mp \boldsymbol{a}\cdot\boldsymbol{V}_r} G_{\alpha_\pm}(-\lambda_\pm(\mathbf{1}_d \times \boldsymbol{a})_X), \\ n^{or\pm} &= N^{or\pm} e^{\mp\phi \pm \boldsymbol{a}\cdot\boldsymbol{V}_r} G_{\alpha_\pm}(+\lambda_\pm(\mathbf{1}_d \times \boldsymbol{a})_X), \\ n^{il\pm} &= n^{ol\pm} \nu e^{2\boldsymbol{a}\cdot\boldsymbol{V}_d}, \\ n^{ir\pm} &= n^{or\pm} \nu e^{2\boldsymbol{a}\cdot\boldsymbol{V}_d}, \end{aligned} \tag{1}$$

with $\nu = n^i(0)/n^o(0) = N^{il\pm}/N^{ol\pm} = N^{ir\pm}/N^{or\pm}$, and where N^{ol+}, N^{or+}, N^{ol-}, and N^{or-} remain to be determined from the boundary conditions. The argument of the cutoff function now is proportional to the magnetic potential component normal to the cutoff direction; the transition is therefore centered around the point where the magnetic potential is zero ($X = 0$). The sense of $\mathbf{1}_d$ is not arbitrary but must be chosen such that the cutoff argument sign is consistent with what is called left and right.

Necessary Equilibrium Conditions

We first establish necessary conditions for which an equilibrium TD magnetopause may exist. As will become clear below, this step reduces the parameter space that has to be explored.

Assume a priori that a magnetopause equilibrium can be found that satisfies the boundary conditions; i.e., uniform asymptotic magnetospheric and magnetosheath fields $\boldsymbol{B}^l$ and $\boldsymbol{B}^r$ exist. In order for the densities in equation (1) to have the correct asymptotic behavior the argument of the cutoff function must have opposite signs on either side of the TD; with $(\mathbf{1}_d \times \boldsymbol{a})_X \approx -\mathbf{1}_d \cdot \boldsymbol{B}\, X$ for $X \to \pm\infty$ one finds

$$\begin{aligned} \mathbf{1}_d \cdot \boldsymbol{B}^l &> 0, \\ \mathbf{1}_d \cdot \boldsymbol{B}^r &> 0, \end{aligned} \tag{2}$$

fixing the sense of $\mathbf{1}_d$ that corresponds to the cutoff as defined before.

There are four possibilities for the relative orientation of $\boldsymbol{V}_r$ and the magnetic field vectors. Consider, for instance, the case in which $(\boldsymbol{V}_r \times \boldsymbol{B}^l)_X > 0$ and $(\boldsymbol{V}_r \times \boldsymbol{B}^r)_X > 0$, i.e., $\boldsymbol{a}^l \cdot \boldsymbol{V}_r < 0$ and $\boldsymbol{a}^r \cdot \boldsymbol{V}_r > 0$. Imposing the prescribed ion density at $-\infty$ amounts to

$$\begin{aligned} N^\infty &= [n^{ol+}(-\infty) + n^{or+}(-\infty)]N^\infty \\ &= [N^{ol+} + N^{or+} e^{2\boldsymbol{a}^l\cdot\boldsymbol{V}_r} \alpha_+]N^\infty \\ &= N^{ol+} N^\infty, \end{aligned}$$

i.e., $N^{ol+} = 1$; from a similar condition at $+\infty$ one finds $N^{or+} = 1$. For the electron density at $-\infty$ one has

$$N^{\infty} = [n^{\mathrm{ol}-}(-\infty) + n^{\mathrm{or}-}(-\infty)]N^{\infty}$$
$$= [N^{\mathrm{ol}-} + N^{\mathrm{or}-}e^{-2\boldsymbol{a}^{\mathrm{l}}\cdot\boldsymbol{V}_{\mathrm{r}}}\alpha_-]N^{\infty}.$$

This result implies that necessarily, $\alpha_- = 0$ and hence that $N^{\mathrm{ol}-} = 1$. From the condition at $+\infty$ one obtains $N^{\mathrm{or}-} = 1$. Analysis of all four possibilities leads to

$$\begin{aligned} N^{\mathrm{ol}+} = N^{\mathrm{or}+} = N^{\mathrm{ol}-} = N^{\mathrm{or}-} = 1, \\ (\boldsymbol{V}_{\mathrm{r}} \times \boldsymbol{B}^{\mathrm{l}})_X > 0 \quad (\boldsymbol{V}_{\mathrm{r}} \times \boldsymbol{B}^{\mathrm{r}})_X > 0 \quad : \quad \alpha_- = 0, \\ (\boldsymbol{V}_{\mathrm{r}} \times \boldsymbol{B}^{\mathrm{l}})_X > 0 \quad (\boldsymbol{V}_{\mathrm{r}} \times \boldsymbol{B}^{\mathrm{r}})_X < 0 \quad : \quad \alpha_{\pm} = 0, \\ (\boldsymbol{V}_{\mathrm{r}} \times \boldsymbol{B}^{\mathrm{l}})_X < 0 \quad (\boldsymbol{V}_{\mathrm{r}} \times \boldsymbol{B}^{\mathrm{r}})_X > 0 \quad : \quad \alpha_{\pm} = 0, \\ (\boldsymbol{V}_{\mathrm{r}} \times \boldsymbol{B}^{\mathrm{l}})_X < 0 \quad (\boldsymbol{V}_{\mathrm{r}} \times \boldsymbol{B}^{\mathrm{r}})_X < 0 \quad : \quad \alpha_+ = 0. \end{aligned} \tag{3}$$

For an ion-dominated layer ($\alpha_- = 1$), only the last case in condition (3) can apply. Electron-dominated layers are described by the first case ($\alpha_+ = 1$). For both types of layers one retrieves the shear flow orientation found by *Sestero* [1966]. The mixed layers ($\alpha_{\pm} = 0$) described by *De Keyser et al.* [1997] allow the four cases.

The inner populations have a nonzero density only within the transition. Their asymptotic density vanishes if $\boldsymbol{a}^{\mathrm{l,r}} \cdot \boldsymbol{V}_{\mathrm{d}} \to -\infty$, or

$$\begin{aligned} \boldsymbol{V}_{\mathrm{d}} \times \boldsymbol{B}^{\mathrm{l}} &> 0, \\ \boldsymbol{V}_{\mathrm{d}} \times \boldsymbol{B}^{\mathrm{r}} &< 0. \end{aligned} \tag{4}$$

This condition generalizes the result found by *Harris* [1962].

The implications of conditions (2) and (4) are illustrated by Figure 4. Since in the proposed model $\boldsymbol{V}_{\mathrm{d}}$ and $\mathbf{1}_{\mathrm{d}}$ are aligned, the strictest of both conditions has to be selected; $\boldsymbol{V}_{\mathrm{d}}$ must lie inside the shaded regions in the figure. When the magnetic field rotates over less than 90°, condition (4) is the strictest one; for larger magnetic field rotation angle, condition (2) is most restrictive. The drift velocity cannot deviate more than 45° from the Y axis.

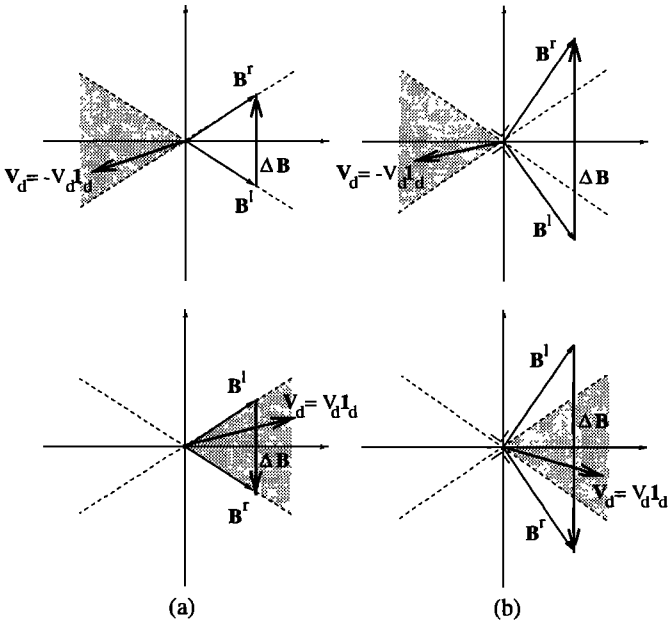

Figure 4. The necessary conditions for the existence of an equilibrium TD magnetopause impose restrictions on the orientation of the diamagnetic drift $\boldsymbol{V}_{\mathrm{d}}$ (equations (2) and (4)); shading indicates the allowed regions. The sign of the drift velocity controls the sense of the magnetic field variation. (a) Magnetic field rotation less than 90°. (b) Magnetic field rotation more than 90°. In either case, $\boldsymbol{V}_{\mathrm{d}}$ deviates at most 45° from the Y axis.

The geometrical consequences of condition (3) depend on the nature of the layer. For ion-dominated layers and mixed transitions with $\alpha_- > 0$, $\alpha_+ = 0$, only the last case in (3) can apply. In Figure 5 the shaded region identifies the allowed $\boldsymbol{V}_{\mathrm{r}}$ orientations; a TD equilibrium exists only if the velocity jump vector lies in this region. Figure 5a shows that $\boldsymbol{V}_{\mathrm{r}}$ must lie in a sector formed by the intersection of two half-planes delineated by $\boldsymbol{B}^{\mathrm{l}}$ and $\boldsymbol{B}^{\mathrm{r}}$. For high magnetic shear this condition enforces $\boldsymbol{V}_{\mathrm{r}} \parallel \Delta\boldsymbol{B}$, as in Figure 5b. The low magnetic shear configuration only implies that $V_{\mathrm{r}z} > 0$ (Figure 5c). The case of electron dominated transitions or mixed layers with $\alpha_- = 0$, $\alpha_+ > 0$ (the first condition in (3)) is similar but with opposite shear flow direction. In the $\alpha_{\pm} = 0$ mixed layer case the cutoffs in the ion and electron VDFs automatically enforce vanishing population density as required; the constraints on the orientation of the velocity difference (and hence the sign of the convection electric field) are then no longer needed.

Computing the TD Equilibrium

We now analyze the Vlasov-Maxwell equations in order to actually compute the electromagnetic structure of the magnetopause. We will assume that $\alpha_+ = 0$; a similar analysis could be carried out for $\alpha_- = 0$. Together, both cases cover all possibilities as indicated by condition (3).

Plasma quasi-neutrality requires that at each point the number of ions (almost) equals the number of electrons. In Appendix A this condition is used to compute the electric potential ϕ. At the center of the transition one finds $\phi(0) = \phi^0$ with $e^{2\phi^0} = 1/(1+\alpha_-)$. Ion-dominated layers ($\alpha_- = 1$) have $\phi^0 = -\frac{1}{2}\ln 2$, while $\alpha_- = 0$ corresponds to $\phi^0 = 0$. If we know the electric potential at $X = 0$, pressure balance between the center of the current layer and the surrounding plasma determines the magnetic field intensity at the center:

$$(B^0)^2 = 1 - \beta^{\infty}[(1+\nu)\sqrt{1+\alpha_-} - 1], \tag{5}$$

where $\beta^{\infty} = 4\mu_0 N^{\infty} kT^{\infty}/(B^{\infty})^2$ is the ratio of kinetic to magnetic pressure far from the TD. As $(B^0)^2 \geq 0$, this sets a limit to the density of the inner populations:

$$\nu \leq \nu_{\max} = \frac{1+\beta^{\infty}}{\beta^{\infty}\sqrt{1+\alpha_-}} - 1. \tag{6}$$

For mixed layers with $\alpha_{\pm} = 0$ one obtains $\nu \leq 1/\beta^{\infty}$. For ion-dominated or mixed layers with $\alpha_+ = 0$, $\alpha_- > 0$ the fact that $\nu \geq 0$ imposes a limit on β^{∞}:

$$\beta^{\infty} \leq \beta^{\infty}_{\max} = \frac{1}{\sqrt{1+\alpha_-} - 1}. \tag{7}$$

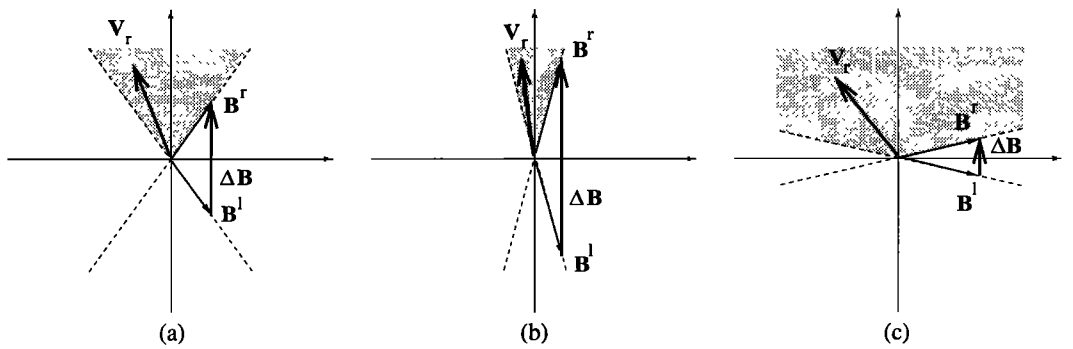

Figure 5. The necessary existence conditions for ion-dominated transitions and mixed layers with $\alpha_+ = 0$, $\alpha_- > 0$ (last case in equation (3)) state that a magnetopause TD equilibrium can exist only when the velocity jump vector is inside the shaded region. Note that the sign of $\boldsymbol{\Delta B}$ does not affect these conditions; rather, it is the sign of B_Y that matters. (a) The general case. (b) Large magnetic shear: $\boldsymbol{V}_r$ is almost aligned with $\boldsymbol{\Delta B}$. (c) Low magnetic shear: $\boldsymbol{V}_r$ lies in the upper quadrants. For the case of electron-dominated transitions and layers with $\alpha_+ > 0$, $\alpha_- = 0$, the necessary conditions require the sign of $\boldsymbol{V}_r$ to be opposite. For mixed layers with $\alpha_\pm = 0$ there are no constraints on the direction of $\boldsymbol{V}_r$.

It is not surprising that such a limitation exists: the ion (and electron) density at the center is $(1 + \nu)\cosh\phi^0$, implying a density enhancement when $\phi^0 \neq 0$ or $\nu > 0$. Limitation (7) amounts to requiring that the kinetic pressure increase does not exceed the available magnetic pressure. For an ion-dominated layer ($\alpha_- = 1$), $\beta^\infty_{\max} = \sqrt{2} + 1 \approx 2.41$; the limit increases as α_- becomes smaller.

Maxwell's equations relate the electric and magnetic field in the magnetopause to the partial currents $\boldsymbol{j}(X)$. Analytical expressions for these currents are found by integrating charge times velocity over all particles of each population [*Roth et al.*, 1996]. The integration procedure is easiest in a reference frame (x, y, z) obtained by rotating (X, Y, Z) in the TD plane so as to align the positive y axis with $\mathbf{1}_d$. Maxwell's equations can be written as a system of three nonlinear second-order ordinary differential equations (ODEs): Ampère's law for the magnetic vector potential components and Poisson's equation for the electric potential. The latter can be replaced by the nonlinear algebraic quasi-neutrality condition, which is a very good approximation [*Roth et al.*, 1990]. This condition allows us to compute $\phi(\boldsymbol{a})$ and to eliminate it from the remaining ODE system:

$$a_y'' + \beta^\infty[\frac{V_{ry}}{2}Q(\boldsymbol{a}) + V_{dy}\bar{Q}(\boldsymbol{a})] = 0, \quad (8)$$

$$a_z'' + \beta^\infty[\frac{V_{rz}}{2}Q(\boldsymbol{a}) + \hat{Q}(\boldsymbol{a})] = 0, \quad (9)$$

with the functions Q, $\bar{Q}$, and $\hat{Q}$ as defined in Appendix A; this appendix presents a more detailed discussion of the above equations. A solution of the ODE system can be computed numerically as follows. From the pressure balance (5) one obtains B^0. Using as initial conditions $\boldsymbol{a}(0) = \mathbf{0}$ and $\boldsymbol{a}'(0) = B^0 \cdot (\sin\theta^0, -\cos\theta^0)$, where θ^0 is the angle $\boldsymbol{B}^0$ makes with the y axis, we can trace the solution backward to $-\infty$ and forward to $+\infty$ until the currents become negligible ($\boldsymbol{a}'' \approx 0$). There is, however, no guarantee that this will happen. In general, for increasing V_r a critical value is reached beyond which the currents do not vanish, and the magnetic field no longer attains a constant asymptotic value.

All computations presented in this paper are carried out in the (x, y, z) frame, in which $\boldsymbol{V}_d$ (or $\mathbf{1}_d$) is along y. From the computed magnetic field profile one can find the direction of the bisectrix of the asymptotic fields, i.e., the direction of the Y axis. This process allows the results obtained in the (x, y, z) frame to be transformed to the (X, Y, Z) frame. In general, both reference frames do not coincide, and therefore $\boldsymbol{V}_d$ (and $\mathbf{1}_d$) is not along Y.

Figure 6 shows a symmetric high magnetic shear configuration that is representative for the dayside magnetopause in the presence of a low-latitude boundary layer: $N^\infty = 15\ \text{cm}^{-3}$, $T^\infty = 5 \times 10^6$ K, $B^\infty = 51$ nT, $\beta^\infty = 2$, $\alpha_\pm = 0$, $\mathcal{L}_+ = 2\rho^+$, $\mathcal{L}_- = \rho^+$, $\rho^+ = 59$ km, and $V_{th}^+ = 287\ \text{km s}^{-1}$. In this computation we have chosen $\boldsymbol{V}_r$ parallel to the z axis. The model asserts that such a relative velocity gives rise to currents in the z direction only (see Appendix A), thus causing B_y variations in the transition. The drift velocity $\boldsymbol{V}_d$ (and hence also $\mathbf{1}_d$) was taken to be along the y axis; the associated y current leads to the B_z reversal. The net result is a symmetric hodogram (Figure 6b): the y axis is the bisectrix of $\boldsymbol{B}^{msph}$ and $\boldsymbol{B}^{msh}$, and the (x, y, z) and (X, Y, Z) frames coincide. The computation was performed for $\boldsymbol{V}_d = (0.5V_{th}^+, 0)$ and $\boldsymbol{V}_r = (0, -V_{th}^+)$; if we neglect magnetospheric flow, this velocity jump corresponds to the magnetosheath flow expected at southern latitude, duskward from the noon meridian. Figure 6b displays a sequence of magnetic field hodograms for increasing velocity difference. From $V_{rz} = -1.1V_{th}^+$ on, no valid solution can be found. Appendix A shows that the magnetic field hodogram at the center of the magnetopause has a parabolic shape. The curvature of the parabola changes with increasing velocity difference, as can be seen in Figure 6b. This parabolic shape has been observed at TD magnetopause crossings [e.g., *Berchem and Russell*, 1982b] as well as in the heliospheric current sheet [e.g., *Behannon et al.*, 1981]

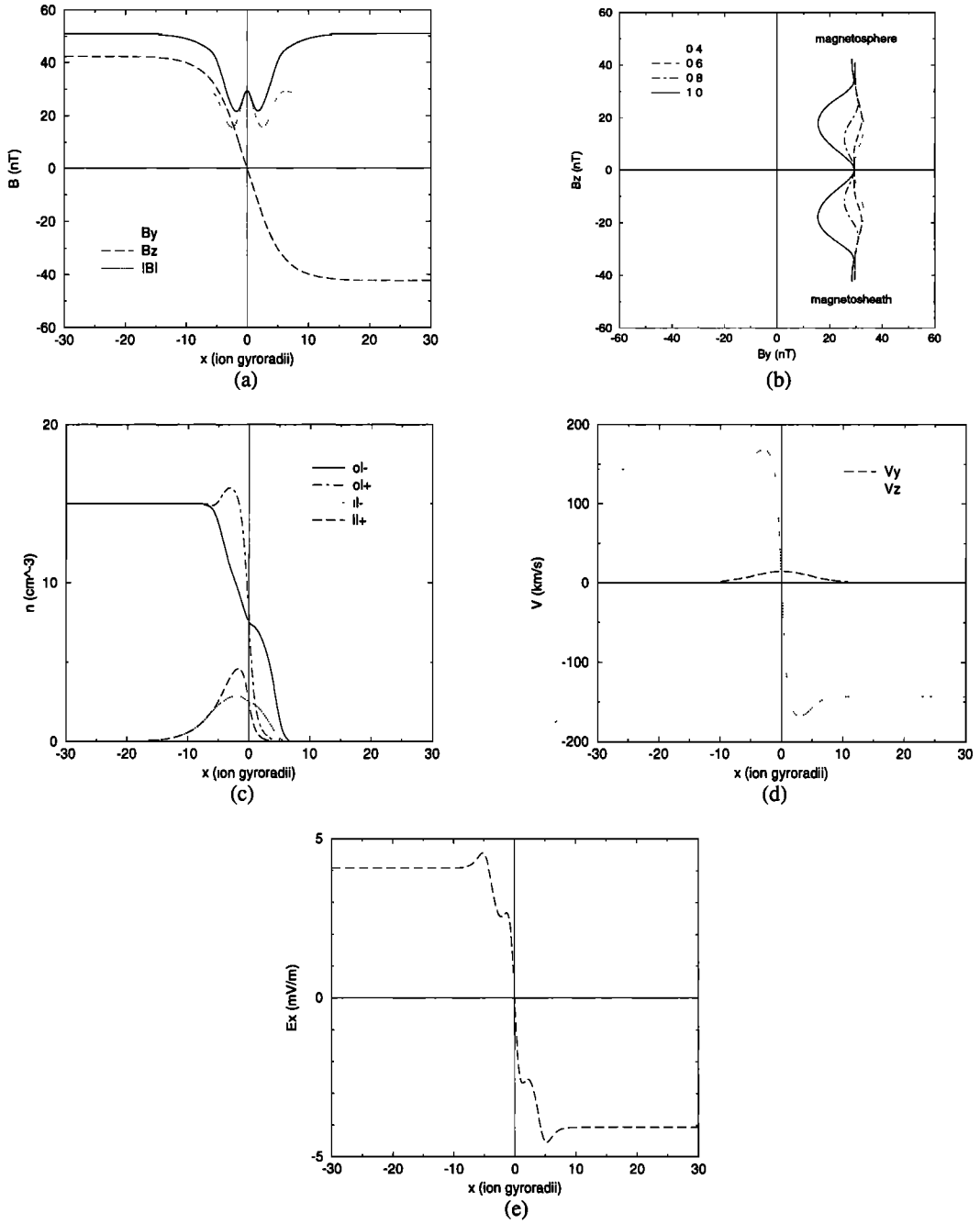

Figure 6. Symmetric high magnetic shear dayside magnetopause configuration at southern latitude: $N^{\infty} = 15$ cm^{-3}, $T^{\infty} = 5 \times 10^6$ K, $B^{\infty} = 51$ nT, $\beta^{\infty} = 2$, $\alpha_{\pm} = 0$, $\mathcal{L}_+ = 2\rho^+$, $\mathcal{L}_- = \rho^+$, $\boldsymbol{V}_{\rm d} = (0.5, 0)V_{\rm th}^+$, and $\boldsymbol{V}_{\rm r} = (0, -1)V_{\rm th}^+$ (the (x, y, z) and (X, Y, Z) frames coincide). The proton gyroradius in the asymptotic field is 59 km; the thermal velocity is $V_{\rm th}^+ = 287$ km s^{-1}. (a) Magnetic field profile. (b) Magnetic field hodograms for increasing relative velocities $V_{rZ} = 0.4 - 1.0V_{\rm th}^+$. (c) Densities of the magnetospheric populations. (d) Plasma bulk velocity. (e) Electric field.

and in solar wind TDs [e.g., *De Keyser et al.*, 1997]. The densities are plotted in Figure 6c, illustrating how inner populations are confined within the current layer, while outer populations cannot penetrate far into the opposite side of the transition. The bulk velocity profile (Figure 6d) is directly related to the ion density profile because of the high proton/electron mass ratio. The y velocity component is due to the drifting inner ions. The sign of the electric field (Figure 6e) inside the layer is largely determined by the asymptotic convection electric field.

Appendix A shows that $B_y(x)$ and $B_z(x)$ are even when the inner populations are absent: the magnetic field may rotate within the transition layer, but the net rotation must be zero regardless of the precise nature of the transition (re-

gardless of $\alpha_\pm$ and $\lambda_\pm$). If, additionally, $\boldsymbol{V}_\mathrm{r} \perp \boldsymbol{B}^\infty$, the magnetic field remains parallel to the y axis throughout the transition as in the *Sestero* [1966] configuration.

Appendix A also presents an analysis for the case in which the relative velocity is small and the layer is dominated by the drift current. The particular case of a dense current sheet embedded in a tenuous plasma (large ν) corresponds to a magnetic field reversal ($|\theta|$ close to 180°) [*Kuznetsova et al.*, 1994]. The transition width then is determined by the Harris length.

Sufficient Equilibrium Conditions

For the particular case $V_{\mathrm{r}y} = 0$, when the (x, y, z) and (X, Y, Z) frames coincide, we are able to establish an approximate sufficient condition. We refer to Appendix B for an alternative, more rigorous derivation of this sufficient condition. Subsequently, for some typical cases, numerical simulation is used to outline the whole set of relative velocities that lead to an equilibrium.

Consider the Vlasov-Maxwell equations near the center of the transition (see Appendix A, equations (A3) and (A4)). Define

$$\zeta^2 = \beta^\infty(1+\nu)\sqrt{1+\alpha_-}|V_{\mathrm{r}z}(\hat{V}_\mathrm{r} + V_{\mathrm{r}z})|/2,$$

with $\hat{V}_\mathrm{r}$ given by

$$\hat{V}_\mathrm{r} = \frac{2}{\sqrt{\pi}}(\lambda_- \frac{1-\alpha_-}{1+\alpha_-} - \lambda_+). \tag{10}$$

Equation (A4) then becomes

$$a_z'' + \mathrm{sign}\,(V_{\mathrm{r}z}(\hat{V}_\mathrm{r} + V_{\mathrm{r}z}))\zeta^2 a_z = 0.$$

If the sign of the coefficient of the second term is negative, the solution behaves like

$$B_y(x) \approx B_y^0 \cosh \zeta x, \quad B_z(x) \approx -\nu\beta^\infty V_{\mathrm{d}y} x;$$

otherwise,

$$B_y(x) \approx B_y^0 \cos \zeta x, \quad B_z(x) \approx -\nu\beta^\infty V_{\mathrm{d}y} x.$$

For the former case, and if $V_{\mathrm{r}y} = 0$, Appendix B shows that the B_y component usually tends to a uniform asymptotic value, where B_y^∞ has the same sign as B_y^0; a solution matching the boundary conditions then exists. In the latter case the B_y component may oscillate, depending on the range of validity of the approximation.

The condition $V_{\mathrm{r}z}(\hat{V}_\mathrm{r} + V_{\mathrm{r}z}) \le 0$ leads, for $\alpha_+ = 0$ and $\alpha_- = 0$, to

$$\begin{array}{llll} B_y^0 > 0 & \mathcal{L}_+ \ge \mathcal{L}_- & -\hat{V}_\mathrm{r} \le V_{\mathrm{r}z} \le 0, \\ B_y^0 > 0 & \mathcal{L}_+ \le \mathcal{L}_- & 0 \le V_{\mathrm{r}z} \le -\hat{V}_\mathrm{r}, \\ B_y^0 < 0 & \mathcal{L}_+ \ge \mathcal{L}_- & 0 \le V_{\mathrm{r}z} \le \hat{V}_\mathrm{r}, \\ B_y^0 < 0 & \mathcal{L}_+ \le \mathcal{L}_- & \hat{V}_\mathrm{r} \le V_{\mathrm{r}z} \le 0, \end{array} \tag{11}$$

while for $\alpha_+ = 0$ and $\alpha_- > 0$ the necessary conditions (the last of equation (3)) fix the sign of $V_{\mathrm{r}z}$, and one finds

$$\begin{array}{ll} B_y^0 > 0 & 0 \le V_{\mathrm{r}z} \le \max\{0, -\hat{V}_\mathrm{r}\}, \\ B_y^0 < 0 & \min\{0, -\hat{V}_\mathrm{r}\} \le V_{\mathrm{r}z} \le 0. \end{array} \tag{12}$$

Similar conditions can be established for the case in which $\alpha_+ > 0$ and $\alpha_- = 0$. From the above analysis we can conclude the following:

1. There exists a limit value $V_\mathrm{r}^{\max}$ beyond which no equilibrium solution can be found. Numerical simulation shows that $|\hat{V}_\mathrm{r}|$ is a lower bound for $V_\mathrm{r}^{\max}$. Conditions (11) and (12) therefore are sufficient existence conditions. This result generalizes *Sestero*'s [1966] conclusion for ion and electron dominated layers that the limit is of the order of the thermal velocity to the case of mixed layers, and it quantifies the influence of the transition lengths.

2. For a given magnetic field variation there exists a preferential orientation for the relative velocity, the sense of which depends on the sign of B_y^∞ and on the characteristic lengths $\mathcal{L}_+$ and $\mathcal{L}_-$.

The above conclusions are illustrated by the diagrams in Figure 7. These diagrams outline the domain of relative velocities $\boldsymbol{V}_\mathrm{r}$ (the shaded region in each diagram) for which a solution can be found, for ion-dominated layers ($\alpha_+ = 0$, $\alpha_- = 1$, $\mathcal{L}_+ = 5\rho^+$) and mixed layers ($\alpha_\pm = 0$, cases $\mathcal{L}_+ = \mathcal{L}_- = 5\rho^+$, $\mathcal{L}_+ = 5\rho^+ > \mathcal{L}_- = \rho^+$, and $\mathcal{L}_+ = \rho^+ < \mathcal{L}_- = 5\rho^+$), with typical parameters $\beta^\infty = 2$, $\theta^0 = 0°$, $V_\mathrm{d} = 0.5V_{\mathrm{th}}^+$, fixing the inner population density by choosing $\nu = \nu_{\max}/2$, and always taking $B_y^\infty > 0$. Two criteria were used to identify unphysical solutions. First, when the relative velocity increases, a point may be reached where the rotation angle starts to vary abruptly, or the angle may not be defined at all if the field does not reach uniform asymptotic values. Second, magnetic field profiles with too many irregular variations and strong gradients are discarded, although they may be valid solutions in the mathematical sense.

For the ion-dominated layers considered in Figure 7a, $\beta^\infty = 2$ is close to $\beta_{\max}^\infty$; equation (6) implies that the inner particle density cannot be large, and hence the magnetic field rotation angle is rather small. A consequence of the necessary conditions is that the relative velocity domain allows only $V_{\mathrm{r}Z} > 0$. For the mixed layers considered in Figures 7b, 7c, and 7d, however, all relative velocity orientations are allowed, although a preference for a particular orientation is evident. Table 1 lists the velocity limits observed along the Z axis and compares them with the sufficient conditions (11) and (12); the sufficient conditions predict the extent of the relative velocity domain along the Z axis rather well. Note that $\hat{V}_\mathrm{r}$ does not depend on β^∞; numerical experiments indicate that the true velocity limit is not very sensitive to β^∞. The diagrams in Figures 8 and 9 offer a different view: they outline the relative velocity domains compatible with 45° and 90° rotations. The problem in constructing these diagrams is to find ν, $\boldsymbol{V}_\mathrm{r}$ combinations that yield the prescribed rotation. These diagrams again show the preferential relative velocity direction; the larger the rotation angle, the more $\boldsymbol{V}_\mathrm{r}$ and $\boldsymbol{\Delta B}$ are aligned.

Sestero [1966] gave a physical explanation for the presence of a relative velocity limit in the case of plasma mo-

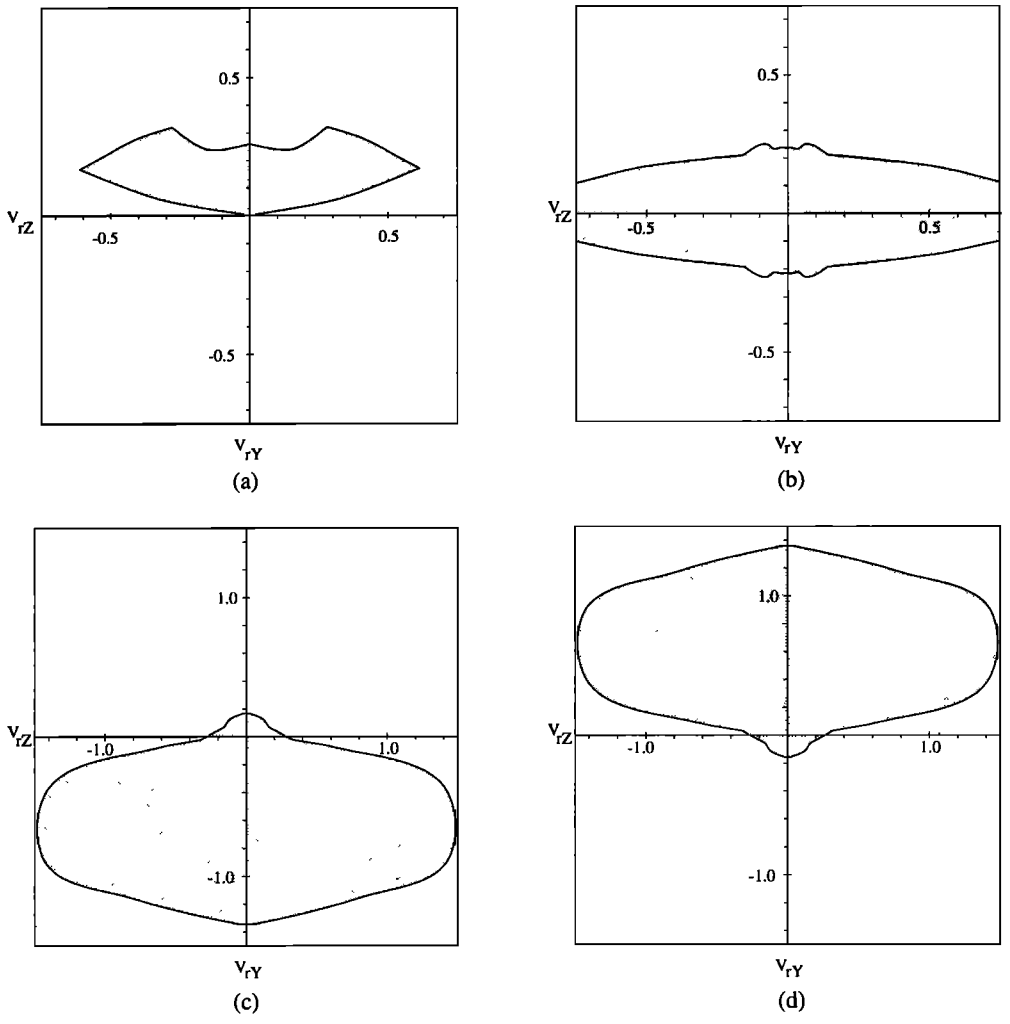

Figure 7. The shaded region in the (Y, Z) plane is the domain of relative velocities $\boldsymbol{V}_r$ (normalized to the proton thermal velocity) for which an equilibrium TD configuration can be found with $\beta^\infty = 2$, $\nu = \nu_{max}/2$, $V_d = 0.5V_{th}^+$, and $\theta^0 = 0°$. (a) Ion-dominated layers with $\mathcal{L}_+ = 5\rho^+$. (b) Mixed layers with $\alpha_\pm = 0$, $\mathcal{L}_\pm = 5\rho^+$. (c) Mixed layers with $\alpha_\pm = 0$, $\mathcal{L}_+ = 5\rho^+$, and $\mathcal{L}_- = \rho^+$. (d) Mixed layers with $\alpha_\pm = 0$, $\mathcal{L}_+ = \rho^+$, and $\mathcal{L}_- = 5\rho^+$.

Table 1. Verification of Sufficient Existence Conditions

α_+	α_-	$\mathcal{L}_+(\rho^+)$	$\mathcal{L}_-(\rho^+)$	Sufficient Condition	True Limit
0	1	5		[0 , 0.23]	[0 , 0.27]
0	1/2	5	5	[0 , 0.15]	[0 , 0.23]
0	1/2	5	1	[0 , 0]	[0 , 0.23]
0	1/2	1	5	[0 , 1.05]	[0 , 1.35]
0	0	5	5	[0 , 0]	[-0.22 , 0.22]
0	0	5	1	[-0.90 , 0]	[-1.35 , 0.17]
0	0	1	5	[0 , 0.90]	[-0.17 , 1.35]
1/2	0	5	5	[-0.15 , 0]	[-0.23 , 0]
1/2	0	5	1	[-1.05 , 0]	[-1.35 , 0]
1/2	0	1	5	[0 , 0]	[-0.23 , 0]
1	0		5	[-0.23 , 0]	[-0.27 , 0]

The domain of relative velocities V_{rZ} (considering only $\boldsymbol{V}_r \parallel Z$) for which an equilibrium exists was predicted using the sufficient condition (11) for $\alpha_\pm = 0$, condition (12) for $\alpha_+ = 0$, $\alpha_- > 0$, and an analogous condition for $\alpha_+ > 0$, $\alpha_- = 0$. There is a good agreement with the existence domain obtained from simulations. The verification was done for the case $\beta^\infty = 2$, $\nu = \nu_{max}/2$, $V_d = 0.5V_{th}^+$, and $\theta^0 = 0°$; the reference frame was chosen such that $B_Y > 0$.

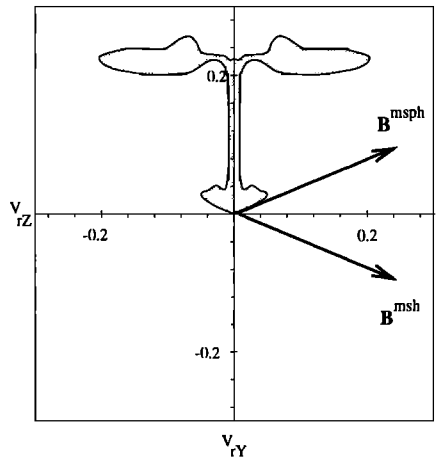

Figure 8. The shaded region in the (Y, Z) plane is the domain of relative velocities $\boldsymbol{V}_r$ (normalized to the proton thermal velocity) for which an ion-dominated magnetopause configuration ($\beta^\infty = 2$, $V_d = 0.5V_{th}^+$, $\theta^0 = 0°$, and $\mathcal{L}_+ = 5\rho^+$) can be found with magnetic field rotation angle $|\theta| = 45°$. The magnetospheric and magnetosheath field vectors are also shown. The same domain is found regardless of the sign of θ.

tion across a unidirectional magnetic field (no magnetic field rotation, $V_{ry} = 0$, $B_z \equiv 0$). A proton or electron with thermal energy $2kT$ crossing a layer with a thickness of the order of a gyroradius must overcome an energy barrier ρeE. Roughly estimating the electric field E in the transition by the convection electric field $V_r B^\infty$, he obtained $V_r < 2kT/\rho eB^\infty = V_{th}$.

Particle Penetration Depths

We define the particle penetration depth of a magnetospheric (magnetosheath) population as the distance at which its density on the magnetosheath (magnetosphere) side of the transition is reduced by a factor $\kappa = 10^{-2}$. The analysis is made here for the magnetospheric populations in a magnetopause of mixed type with $\alpha_\pm = 0$, $B_y^r > 0$ and $B_z^r > 0$. The angle between $\boldsymbol{B}^r$ and the y axis is denoted by θ^r. It is not easy to obtain an analytical estimate of the penetration depth of a particular population. Indeed, the number densities in equation (1) depend on ϕ and $\boldsymbol{a}$, which are determined by all populations simultaneously. We have therefore studied separately the case in which the current is mainly carried by the inner populations (transition dominated by the drift current) and the case in which the outer populations contribute most to the total current (currents due to the velocity shear).

For a mixed layer where the drift current dominates the transition ($V_{ry} = 0$, V_{rz} small) we find in Appendix A (see equations (A7 and (A9)) that a reduction by a factor κ corresponds to a penetration depth

$$x_d \approx \operatorname{acosh}(\kappa^{-1/2})\frac{\mathcal{L}'}{\rho^+} \approx \frac{3\mathcal{L}_d}{\rho^+ \sin\theta^r}. \qquad (13)$$

Simulations show that this penetration depth does not change much in the presence of a moderate relative velocity; the hodograms in Figure 6b also indicate that the rotation angle is not very sensitive to the relative velocity as long as V_r remains well inside the existence domain.

The magnetospheric densities given by equation (1) can be approximated for $x > 0$ by

$$n^{ol\pm} \approx e^{\mp 2\boldsymbol{a}\cdot\boldsymbol{V}_r - \lambda_\pm^2 a_z^2}/2\sqrt{\pi}\lambda_\pm |a_z|.$$

These number densities vanish over a distance controlled by $\lambda_\pm$. The situation $V_{ry} = 0$ is considered in particular; i.e., the velocity difference is along the z axis and $\theta^r = \theta/2$. Define the values $\xi^\pm = -\lambda_\pm a_z$ as the solutions of the nonlinear conditions

$$e^{\pm 2\xi V_{rz}/\lambda_\pm - \xi^2}/2\sqrt{\pi}\xi = \kappa. \qquad (14)$$

When B_y^r is not too small, i.e., $|\theta|$ not close to 180°, the approximation $a_z \approx -B_y^r x$ is reasonable, and the penetration depths of magnetospheric ions and electrons are

$$x_\pm \approx \frac{\xi^\pm}{\lambda_\pm \cos\theta^r}. \qquad (15)$$

As $|V_{rz}/\lambda|$ cannot be much larger than 1 (as dictated by the sufficient conditions (11) and (12) and by equation (10)), one finds that the largest of ξ^+ and ξ^- is ≈ 3.

Inspection of equation (14) reveals that $\xi^+(V_{rz}/\lambda)$ is a monotonously increasing function. Moreover, when $\lambda \approx \lambda_+ \approx \lambda_-$, one has $\xi^+(V_{rz}/\lambda) \approx \xi^-(-V_{rz}/\lambda)$. Therefore $\xi^+(|V_{rz}/\lambda|) > \xi^-(|V_{rz}/\lambda|)$. This relation implies that the ion penetration depth is largest when $V_{rz} > 0$; otherwise the electron depth is dominant. This behavior is controlled by the sign of the electric field in the layer: in the former case a positive electric field E_x repels the electrons, and in the latter case a negative E_x prohibits magnetospheric protons from entering the magnetosheath. This finding is illustrated by Figure 6 (a case in which $V_{rz} < 0$): the negative magnetosheath electric field (Figure 6d) repels the protons, which consequently penetrate the magnetosheath but not so far as the electrons, as can be seen from the density profiles in Figure 6c. *Cargill and Eastman* [1991] similarly found, using hybrid simulations of one-dimensional TDs in the presence of transverse flow, that the orientation of the flow influences the transition length scale of the bulk velocity profile. Indeed, the orientation of the flow determines the sign of the electric field inside the transition and, consequently, the ion particle penetration depth and the transition length of the bulk velocity profile.

Asymmetric Plasma Conditions and Proton/Electron Temperature Ratio

The foregoing analysis discussed symmetric transitions with little change in magnetic field magnitude and plasma density and temperature, and with equal proton and electron temperatures. Usually, some degree of asymmetry between magnetosheath and magnetospheric plasma and field properties is present. This is particularly true when a boundary

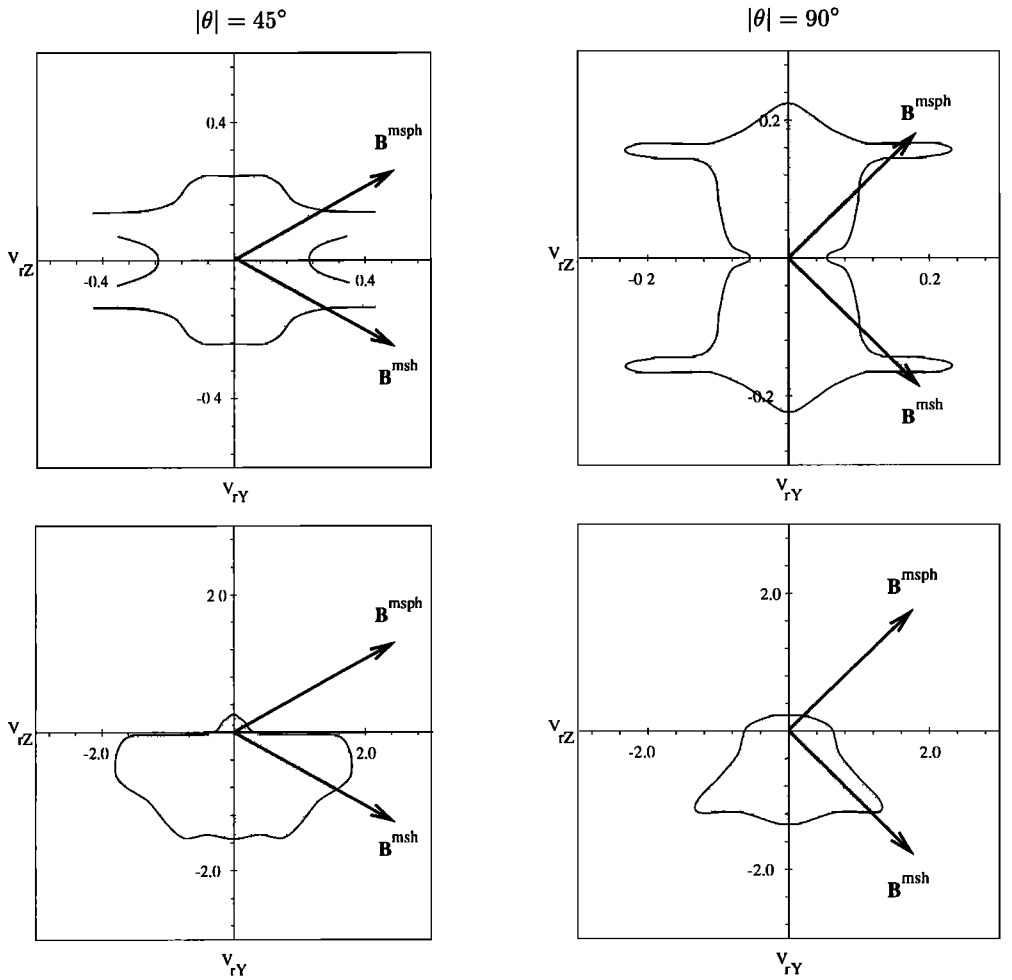

Figure 9. The shaded region in the (Y, Z) plane is the domain of relative velocities $\boldsymbol{V}_r$ (normalized to the proton thermal velocity) for which a mixed layer magnetopause configuration ($\alpha_\pm = 0$, $\beta^\infty = 2$, $V_d = 0.5V_{th}^+$, and $\theta^0 = 0°$) with magnetic field rotation angle (left) $|\theta| = 45°$ and (right) $|\theta| = 90°$ exists, for (top) $\mathcal{L}_\pm = 5\rho^+$, and (bottom) $\mathcal{L}_+ = 5\rho^+$ and $\mathcal{L}_- = \rho^+$; the diagrams for $\mathcal{L}_+ = \rho^+$ and $\mathcal{L}_- = 5\rho^+$ are mirror images of the latter. The magnetospheric and magnetosheath field vectors are sketched. The same domains are found regardless of the sign of θ.

layer is absent [*Eastman et al.*, 1996]. Also, the protons are typically 10 times hotter than the electrons. To assert the generality of the conclusions obtained from the model, simulations have been carried out for more realistic configurations.

Figure 10 shows the simulated structure of a typical southern latitude dayside magnetopause configuration in the absence of a low-latitude boundary layer. The magnetospheric conditions characterize a tenuous hot plasma in the strong geomagnetic field ($N^{\mathrm{msph}} = 0.1$ cm^{-3}, $T^{\mathrm{msph}+} = 20 \times 10^6$ K, $T^{\mathrm{msph}-} = 1 \times 10^6$ K, and $B^{\mathrm{msph}} = 100$ nT). The magnetosheath is relatively dense but colder ($N^{\mathrm{msh}} = 20$ cm^{-3}, $T^{\mathrm{msh}+} = 5 \times 10^6$ K, $T^{\mathrm{msh}-} = 0.75 \times 10^6$ K, and $B^{\mathrm{msh}} = 78$ nT). The magnetopause is modeled as a mixed layer ($\alpha_\pm = 0$, $\mathcal{L}_+^{\mathrm{msph}} = 2\rho^{\mathrm{msph}+}$, $\mathcal{L}_-^{\mathrm{msph}} = \rho^{\mathrm{msph}+}$, $\mathcal{L}_+^{\mathrm{msh}} = 2\rho^{\mathrm{msh}+}$, $\mathcal{L}_-^{\mathrm{msh}} = \rho^{\mathrm{msh}+}$, and $\nu = 1.0$). The magnetosheath proton gyroradius $\rho^{\mathrm{msh}+} = 38$ km is used as the reference length in Figure 10. We have fixed the length scales of the diamagnetic current layer by choosing $\mathcal{L}_d^{\mathrm{msph}} = 3\rho^{\mathrm{msph}+}$ and $\mathcal{L}_d^{\mathrm{msh}} = 3\rho^{\mathrm{msh}+}$. As a consequence of the different gyroradii and the different temperatures of the populations the corresponding drift velocities are different as well. The magnetosheath velocity was taken to be $\boldsymbol{V}_r = (0, -0.20V_{th}^{\mathrm{msh}+}) = (0, -60)$ km/s in the (x, y, z) frame. The plots in Figure 10 are all made in this (x, y, z) frame. The overall structure of the transition is similar to the symmetric case, with inner populations confined to the current layer. The bulk plasma velocity profile is shown in Figure 10e. The electric field (Figure 10f), while being affected by the temperature differences between the populations at the center of the transition, must match the convection electric fields at both ends of the transition.

Although it is not obvious how the conclusions regarding the relative velocity domains for symmetric configurations can be generalized for asymmetric transitions and for the case of different proton and electron temperatures, Fig-

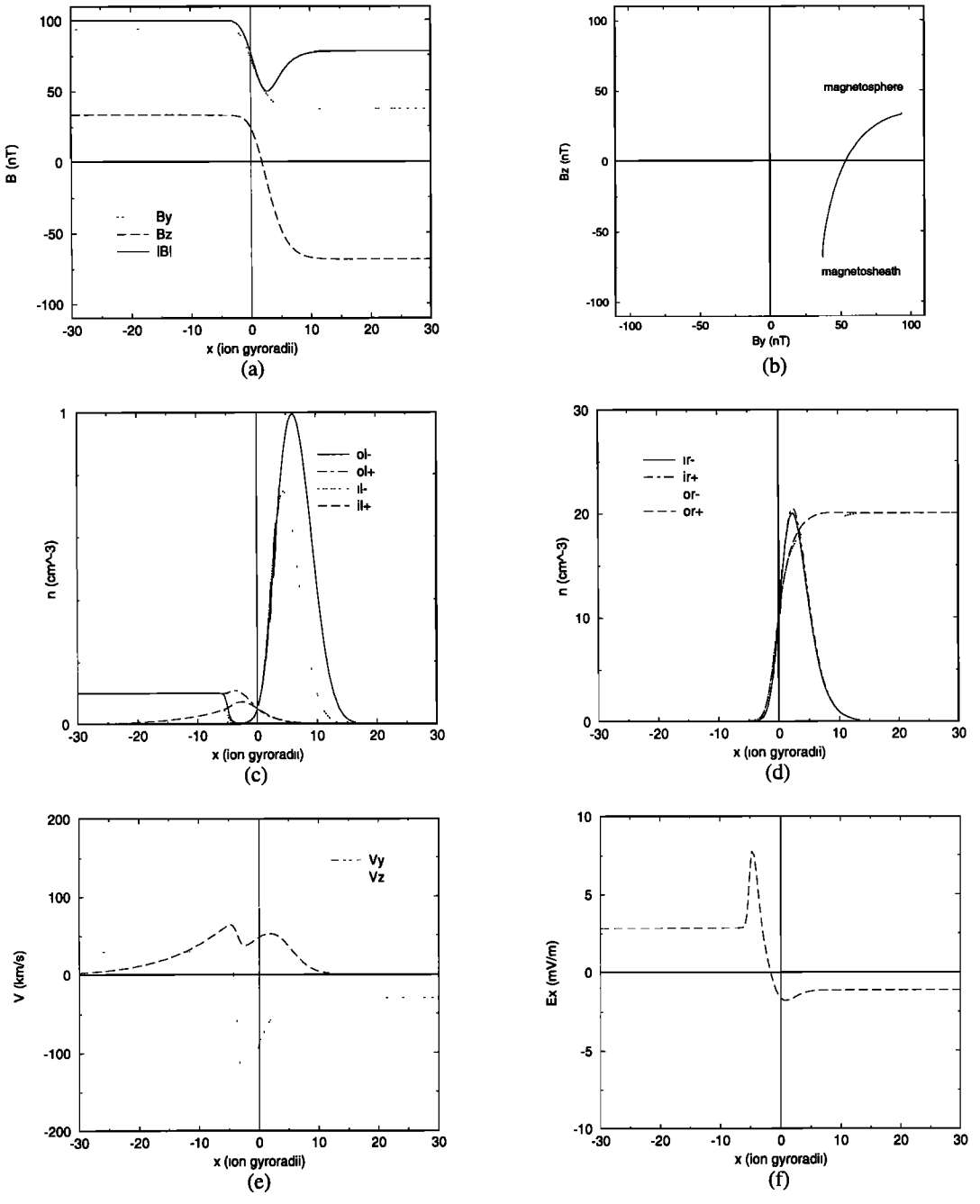

Figure 10. Asymmetric southern latitude magnetopause configuration. Magnetospheric conditions (typical when the low-latitude boundary layer is absent): $N^{\mathrm{msph}} = 0.1$ cm^{-3}, $T^{\mathrm{msph}+} = 20 \times 10^6$ K, $T^{\mathrm{msph}-} = 1 \times 10^6$ K, and $B^{\mathrm{msph}} = 100$ nT. Magnetosheath conditions: $N^{\mathrm{msh}} = 20$ cm^{-3}, $T^{\mathrm{msh}+} = 5 \times 10^6$ K, $T^{\mathrm{msh}-} = 0.75 \times 10^6$ K, and $B^{\mathrm{msh}} = 78$ nT. The magnetosheath proton gyroradius $\rho^{\mathrm{msh}+} = 38$ km is taken as the reference length. The layer is of mixed type: $\alpha_{\pm} = 0$, $\mathcal{L}_{+}^{\mathrm{msph}} = 2\rho^{\mathrm{msph}+}$, $\mathcal{L}_{-}^{\mathrm{msph}} = \rho^{\mathrm{msph}+}$, $\mathcal{L}_{+}^{\mathrm{msh}} = 2\rho^{\mathrm{msh}+}$, $\mathcal{L}_{-}^{\mathrm{msh}} = \rho^{\mathrm{msh}+}$, and $\nu = 1.0$. The scale length of the diamagetic layer was fixed by choosing $\mathcal{L}_{\mathrm{d}}^{\mathrm{msph}} = 3\rho^{\mathrm{msph}+}$ and $\mathcal{L}_{\mathrm{d}}^{\mathrm{msh}} = 3\rho^{\mathrm{msh}+}$. The velocity difference across the TD is $\boldsymbol{V}_{\mathrm{r}} = (0, -0.20)V_{\mathrm{th}}^{\mathrm{msh}+}$, expressed in the (x, y, z) frame. (a) Magnetic field profile. (b) Magnetic field hodogram. (c) Density profiles of the magnetospheric populations. (d) Density profiles of the magnetosheath populations. (e) Plasma bulk velocity. (f) Electric field.

ure 10f shows that also in more realistic simulations the sign of the electric field inside the layer—the essential factor determining the structure of the transition—is determined by the convection electric field (i.e., by the relative orientation of velocity and magnetic field vectors), at least in situations in which the velocity jump is large; large velocities are precisely what we consider here in determining the maximum relative velocity that allows TD equilibrium. Some preference for certain relative velocity directions is therefore expected. When the relative velocity is

small, however, large temperature differences between protons and electrons and/or an important asymmetry between magnetospheric and magnetosheath plasmas predominantly control the structure of the layer.

Implications for the Magnetopause

The magnetopause model described in this paper has led to some important conclusions regarding the preferred orientation of the relative velocity with respect to the magnetic field and regarding the particle penetration depths. These theoretical results are confronted here with a number of published magnetopause observations [*Berchem and Russell*, 1982b; *Paschmann et al.*, 1986; *Eastman et al.*, 1996; *Le and Russell*, 1994; *Phan and Paschmann*, 1996] in order to demonstrate that the model appears consistent with the observations. Such a comparison necessarily suffers from the variability of the magnetopause as a consequence of the ever-changing solar wind and interplanetary magnetic field conditions and the limited coverage (e.g., in latitude) by satellites. To focus on the role of the magnetosheath conditions, we will ignore in this discussion the plasma velocity on the magnetospheric side; the relative velocity then is essentially the magnetosheath flow.

Most Probable Configurations

Figure 11 schematically represents the magnetic field and plasma velocity configuration at the magnetopause. As the magnetosheath plasma is deflected in all directions around the magnetosphere, all possible orientations of the flow with respect to the magnetospheric magnetic field occur. The model can account for all these geometries by assuming that the transition is of the mixed type. Observations of magnetosheath beta up to 30 [*Phan and Paschmann*, 1996] lead (according to equation (7)) to the same conclusion: the transition is mixed as large $\beta_{\max}^{\infty}$ imply small α_{-}. It is expected that the ion characteristic length exceeds the electron length ($\mathcal{L}_{+} \geq \mathcal{L}_{-}$) because of the larger ion gyroradius.

Consider first the high magnetic shear dayside magnetopause (magnetic field rotation angle $90° \leq \theta \leq 180°$). Figures 11a and 11b sketch typical near-noon configurations at northern and southern latitude as seen toward Earth. Going from magnetosphere to magnetosheath, the magnetic field rotates from north to south polarity. If $B_Y > 0$ (Figure 11b), the situation is qualitatively comparable to the $\mathcal{L}_{+} \geq \mathcal{L}_{-}$ cases in Figure 9 (the fact that the rotation angle in that figure is smaller than the typical high shear magnetopause rotation is due to the rather large beta chosen there); the preferential relative velocity direction is southward. If $B_Y < 0$ (Figure 11a), northward relative velocities are preferred. In conclusion, the equilibrium configurations most likely to occur have $B_Y < 0$ in the northern and $B_Y > 0$ in the southern hemisphere, i.e., clockwise magnetic field rotation in the north and counterclockwise rotation in the south. This finding is consistent with the observations reported by *Sonnerup and Cahill* [1968], who show a marked sense-of-rotation difference between both hemispheres for rotational discontinuity magnetopause crossings and, to a lesser degree, a similar effect for tangential discontinuity crossings. Such a difference, however, was not present in the analysis of *Berchem and Russell* [1982b]. According to the TD model, the preference for a particular sense of rotation is absent for small relative velocities (near the stagnation point at

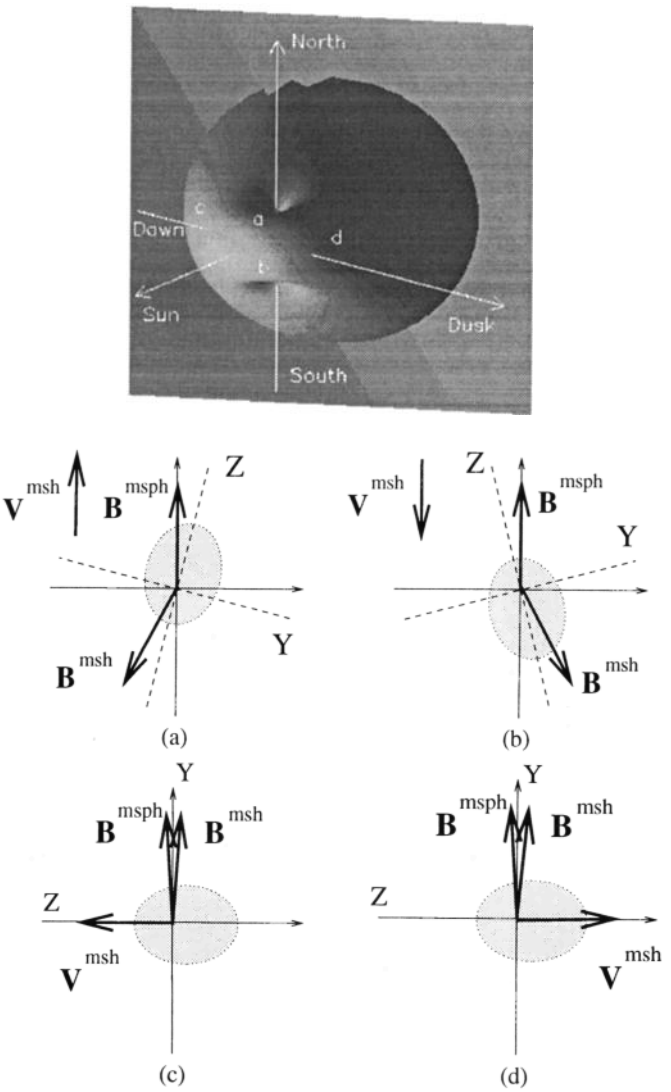

Figure 11. Configurations at different sites marked a–d on the magnetopause surface, as seen toward Earth. The magnetopause is assumed to be a mixed layer ($\mathcal{L}_{+} \geq \mathcal{L}_{-}$). The magnetosheath flow is denoted by $\boldsymbol{V}^{\mathrm{msh}}$; magnetospheric flow is neglected. $\boldsymbol{B}^{\mathrm{msh}}$ and $\boldsymbol{B}^{\mathrm{msph}}$ denote the magnetosheath and magnetospheric fields. Each panel shows the (Y, Z) frame (where Y is along the bisectrix of $\boldsymbol{B}^{\mathrm{msh}}$ and $\boldsymbol{B}^{\mathrm{msph}}$), and the domain of acceptable relative velocities is roughly sketched by the shaded regions. (a) High magnetic shear in the northern hemisphere: northward $\boldsymbol{V}^{\mathrm{msh}}$ is preferred when $B_Y < 0$, or clockwise rotation. (b) High magnetic shear in the southern hemisphere: southward $\boldsymbol{V}^{\mathrm{msh}}$ is preferred when $B_Y > 0$, or counterclockwise rotation. (c) Low magnetic shear at the dawnside: tailward $\boldsymbol{V}^{\mathrm{msh}}$ does not point in the preferential direction; equilibrium may be disrupted for relatively small $\boldsymbol{V}^{\mathrm{msh}}$. (d) Low magnetic shear at the duskside: $\boldsymbol{V}^{\mathrm{msh}}$ points in the preferred direction.

the nose of the magnetopause) and equal transition lengths. It becomes more pronounced as the magnetosheath velocity is larger and only when the proton characteristic length exceeds the electron length. Rather than strictly impose the sense of rotation (as in the RD analysis of *Su and Sonnerup* [1968]), there is only a preference for a particular sense.

A similar argument can be applied to the tail flanks of the magnetopause where the magnetospheric field is parallel (antiparallel) to the magnetosheath flow in the southern (northern) lobe. For high magnetic shear (that is, tailward magnetosheath field in the northern lobe and sunward magnetosheath field in the southern lobe) there is a preference for counterclockwise rotation above and clockwise rotation below the equator.

Figures 11c and 11d show low magnetic shear configurations at the dawn and dusk magnetopause, which are similar to those studied by *Sestero* [1966]. At the dawnside and duskside the magnetosheath velocity is significant. It can be seen that the magnetosheath flow is in the preferred direction at the duskside; it has the opposite direction at the dawnside. TD equilibrium is therefore expected to be lost more easily at the dawnside, a result that agrees with the analysis of *Wu* [1986b].

Magnetopause Thickness

A rough estimate of the magnetopause current layer half-thickness D can be obtained by considering the penetration depths (see equations (13) and (15)) of those populations that significantly contribute to the current. For large magnetic field rotation angle ($|\theta|$ close to 180°) the drift current due to the inner populations dominates the transition. For small $|\theta|$ the drift current is negligible. For intermediate rotation angles, both the outer and the inner populations significantly contribute to the current. A crude thickness estimate therefore is

$$\begin{array}{ll} D \approx 3\max\{\mathcal{L}_\pm\} & |\theta| \text{ small}, \\ D \approx 3\max\{\frac{\mathcal{L}_d}{\sin(\theta/2)}, \frac{\mathcal{L}_\pm}{\cos(\theta/2)}\} & |\theta| \text{ intermediate}, \\ & V_{ry} = 0, V_{rz} \text{ small}, \\ D \approx 3\mathcal{L}_d & |\theta| \text{ close to } 180°. \end{array} \quad (16)$$

The ranges in which these approximations apply depend on the relative importance of the currents carried by inner and outer populations.

Consider mixed layers where $\mathcal{L}_d$ and the ion transition length $\mathcal{L}_+$ are the same, i.e., layers characterized by a single length parameter $\delta = \mathcal{L}_d = \mathcal{L}_+$ (it is assumed that $\mathcal{L}_+ \geq \mathcal{L}_-$ and $\xi^+ \approx 3$). Figure 12 plots the magnetopause current layer thickness obtained with equation (16) for layers with δ ranging from 1 to 3 ion gyroradii. The estimated thicknesses seem compatible with observations (compare, for instance, with Figure 8 of *Berchem and Russell* [1982a]), although a detailed comparison is difficult because of the large scatter in observational thickness determinations.

It is interesting to note that for low magnetic shear, equation (16) estimates the dusk magnetopause thickness to be $D \approx 3\mathcal{L}_+$ (as $V_{rZ} < 0$; see Figure 11d), while the dawnside magnetopause would be thinner as $D \approx 3\mathcal{L}_-$ ($V_{rZ} > 0$; see Figure 11c).

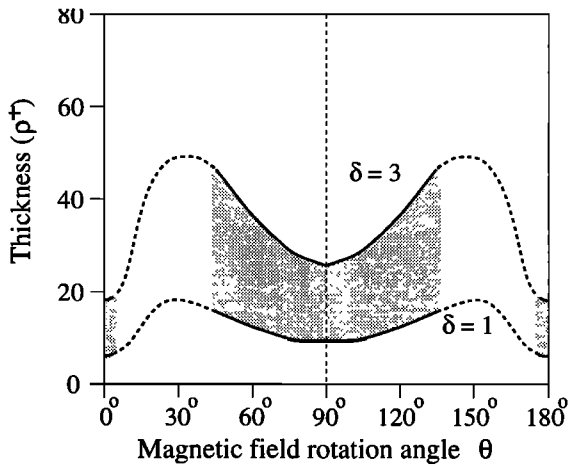

Figure 12. Magnetopause thickness $2D$ (D is the half-thickness estimate of equation (16)) as a function of magnetic field rotation angle θ, for mixed layers ($\alpha_\pm = 0$) characterized by a single length scale $\delta = \mathcal{L}_d = \mathcal{L}^+$ (assuming $\mathcal{L}^+ \geq \mathcal{L}^-$) ranging from 1 to 3 ion gyroradii (ρ^+). The precise range of validity of the thickness estimate is difficult to establish, as it depends on the relative importance of the contributions of inner and outer populations to the total current. The shaded regions indicate the thickness range for small (θ close to 0°), intermediate (assuming $V_{rY} = 0$), and large ($\theta \approx 180°$) rotation angles. The dotted lines are extrapolations where the estimate is not valid.

It should be stressed that the variations in magnetic field, bulk velocity, and number densities do not necessarily occur on the same spatial scale or at the same location. In the symmetric transition shown in Figure 6, for instance, the major change in the plasma bulk velocity takes place in a region that is much thinner than the current layer (i.e., the width as observed in the magnetic field profile): the transition scale of the bulk velocity z component is closely related to the length scale of the outer ion density profile, while the diamagnetic current is carried by a small number of inner particles that are distributed in a relatively wide layer but have little influence on the bulk velocity. In the asymmetric transition in Figure 10 the positions of the magnetic field transition and the bulk velocity jump do not coincide. Since the bulk velocity strongly depends on the mean velocity of the most abundant ion population (i.e., the magnetosheath ions), it is obvious that the main change in bulk velocity is shifted toward the magnetospheric side.

Conclusions

The study presented in this paper is based on an analysis of the role of the relative velocity between the plasmas on either side of a plane tangential discontinuity in equilibrium. It turns out that there is an upper limit to the velocity difference the transition can support; this limit may vary significantly with the velocity jump direction and may even preclude an

equilibrium for some directions. The precise form of the relative velocity domain for which acceptable equilibria exist is strongly affected by the nature of the transition and by the transition lengths. The dominant factor is the sign of the electric field within the current layer (determined by the relative orientation of magnetic field and velocity difference), which constitutes an energy barrier for either the electrons or the ions.

Satellite observations have shown that the magnetopause is an ever-changing, dynamic entity, with both TD- and RD-like behavior. *Su and Sonnerup* [1968] predict a specific sense of magnetic field rotation for the RD magnetopause; the rotation sense above and below the equatorial plane should be opposite. While observations at times have strongly pointed in this direction [*Sonnerup and Cahill*, 1968], they sometimes failed to show the predicted sense as in the study by *Berchem and Russell* [1982b], who ascribed this discrepancy to the incompleteness of the kinetic theory for rotational discontinuities and to the difficulties in interpreting magnetopause observations.

The merit of the present paper lies in the fact that it analyzes the conditions under which a TD magnetopause may exist. For high magnetic shear the results suggest a preferential magnetic field rotation sense depending on the orientation of the plasma velocity jump across the magnetopause, which is mainly determined by the magnetosheath flow. The analysis shows that the rotation sense can be either way but that, at least for large magnetic shear and sufficiently large magnetosheath flow velocity, one rotation sense is preferred. Which sense that is depends on the characteristic transition lengths of the particle populations involved and on the direction of the magnetosheath flow. One recovers the same north-south asymmetry as that found by *Su and Sonnerup* [1968] for rotational discontinuities. At the same time the model leads to an estimate of the magnetopause thickness that appears consistent with in situ observations. For low magnetic shear a dawn-dusk asymmetry is found, with a thicker current layer at the dusk magnetopause. Nonequilibrium seems more probable at the dawnside [see *Wu*, 1986b].

The proposed model obviously has a number of shortcomings. Below we point out to what extent the conclusions depend on the specific assumptions of the model.

First, there are limitations to the kinetic model as such. We had to decide on a specific shape of the velocity distribution functions. Also, assumptions had to be made about the inner populations. In general, only knowledge about the source of these populations could resolve this problem [*Whipple et al.*, 1984]. Although the conclusions regarding the inner populations (zero magnetic field rotation when they are absent, large rotation when there is a dense diamagnetic current sheet) depend on these assumptions, they are qualitatively consistent with other studies [*Harris*, 1962; *Lee and Kan*, 1979]. The model generalizes existing kinetic models and leads to the same generic conclusions: the influence of the relative orientation of magnetic field and velocity difference on the structure of the TD, the role of the nature of the transition and the transition lengths, and a relative velocity limit proportional to the thermal velocity. Note that the analysis presented here refers only to equilibrium solutions; the effect of time variations or instabilities is not investigated. Instabilities (e.g., the Kelvin-Helmholtz instability) may impose additional restrictions on the velocity difference.

Second, a number of simplifications have been made in applying the kinetic model to the magnetopause. For instance, the presence of heavy ions has been ignored, as well as the asymptotic temperature anisotropy of magnetosheath and magnetospheric populations. The effect of a difference in the constant asymptotic values of the electric potential in comoving magnetospheric and magnetosheath frames was not considered. To focus on the effect of the relative velocity, this paper was devoted to symmetric configurations with equal proton and electron temperatures. We discussed briefly the case of asymmetric transitions and different proton and electron temperatures. We concluded that, especially for large relative velocities, the sign of the electric field inside the layer is determined by the orientation of the relative velocity with respect to the magnetic field; this orientation is therefore expected to leave its imprint on the existence conditions of more realistic transitions as well.

The TD model has implications that go beyond the study of the equilibrium magnetopause. It has already been used for the interpretation of solar wind TDs [*De Keyser et al.*, 1997]. The availability of a realistic equilibrium model also forms the starting point for an assessment of the stability of TD transitions [*Kuznetsova et al.*, 1994; *Kuznetsova and Roth*, 1995]. Hence the model may contribute to an improved understanding of the time-dependent behavior of TDs.

Appendix A: Vlasov-Maxwell Equations

The Vlasov-Maxwell equations describing TD equilibrium are derived below in their dimensionless form. Define the auxiliary functions

$$\begin{aligned} f_\lambda(\boldsymbol{a}, \boldsymbol{V}_\mathrm{r}) &= 1 - \mathrm{erf}(\lambda a_z)\tanh(\boldsymbol{a}\cdot\boldsymbol{V}_\mathrm{r}), \\ \hat{f}_\lambda(\boldsymbol{a}, \boldsymbol{V}_\mathrm{r}) &= 1 + \mathrm{erf}(\lambda a_z)\tanh(\boldsymbol{a}\cdot\boldsymbol{V}_\mathrm{r}), \\ g_\lambda(\boldsymbol{a}, \boldsymbol{V}_\mathrm{r}) &= 1 - \mathrm{erf}(\lambda a_z)\coth(\boldsymbol{a}\cdot\boldsymbol{V}_\mathrm{r}), \\ \hat{g}_\lambda(\boldsymbol{a}, \boldsymbol{V}_\mathrm{r}) &= 1 + \mathrm{erf}(\lambda a_z)\coth(\boldsymbol{a}\cdot\boldsymbol{V}_\mathrm{r}). \end{aligned}$$

The quasi-neutrality condition leads to the following expression for the electric potential:

$$e^{2\phi} = \frac{f_{\lambda_+}(\boldsymbol{a}, \boldsymbol{V}_\mathrm{r})}{2\alpha_- + (1-\alpha_-)\hat{f}_{\lambda_-}(\boldsymbol{a}, \boldsymbol{V}_\mathrm{r})}.$$

Because $\boldsymbol{V}_\mathrm{d}^+ = -\boldsymbol{V}_\mathrm{d}^-$, and because the same ν is used for all inner populations, the electric potential does not depend explicitly on ν or V_d. Note that in the dimensionless notation, $\phi(\pm\infty) = \pm\boldsymbol{a}(\pm\infty)\cdot\boldsymbol{V}_\mathrm{r}$. With the partial currents (moments of first order),

$$
\begin{aligned}
j_y^{\mathrm{lo}\pm} &= \mp\frac{V_{\mathrm{ry}}}{2} e^{\mp\phi\mp\boldsymbol{a}\cdot\boldsymbol{V}_{\mathrm{r}}} G_{\alpha_\pm}(-\lambda_\pm a_z),\\
j_y^{\mathrm{li}\pm} &= \mp\nu(\frac{V_{\mathrm{ry}}}{2} \mp V_{\mathrm{dy}}) e^{\mp\phi\mp\boldsymbol{a}\cdot\boldsymbol{V}_{\mathrm{r}}+2\boldsymbol{a}\cdot\boldsymbol{V}_{\mathrm{d}}} G_{\alpha_\pm}(-\lambda_\pm a_z),\\
j_y^{\mathrm{ro}\pm} &= \pm\frac{V_{\mathrm{ry}}}{2} e^{\mp\phi\pm\boldsymbol{a}\cdot\boldsymbol{V}_{\mathrm{r}}} G_{\alpha_\pm}(+\lambda_\pm a_z),\\
j_y^{\mathrm{ri}\pm} &= \pm\nu(\frac{V_{\mathrm{ry}}}{2} \pm V_{\mathrm{dy}}) e^{\mp\phi\pm\boldsymbol{a}\cdot\boldsymbol{V}_{\mathrm{r}}+2\boldsymbol{a}\cdot\boldsymbol{V}_{\mathrm{d}}} G_0(+\lambda_\pm a_z),\\
j_z^{\mathrm{lo}\pm} &= e^{\mp\phi\mp\boldsymbol{a}\cdot\boldsymbol{V}_{\mathrm{r}}}\cdot\\
&\qquad [\mp\frac{V_{\mathrm{rz}}}{2} G_{\alpha_\pm}(-\lambda_\pm a_z) + \frac{\lambda_\pm}{2\sqrt{\pi}}(1-\alpha_\pm) e^{-\lambda_\pm^2 a_z^2}],\\
j_z^{\mathrm{li}\pm} &= \nu e^{2\boldsymbol{a}\cdot\boldsymbol{V}_{\mathrm{d}}} j_z^{\mathrm{lo}\pm},\\
j_z^{\mathrm{ro}\pm} &= e^{\mp\phi\pm\boldsymbol{a}\cdot\boldsymbol{V}_{\mathrm{r}}}\cdot\\
&\qquad [\pm\frac{V_{\mathrm{rz}}}{2} G_{\alpha_\pm}(+\lambda_\pm a_z) - \frac{\lambda_+}{2\sqrt{\pi}}(1-\alpha_\pm) e^{-\lambda_\pm^2 a_z^2}],\\
j_z^{\mathrm{ri}\pm} &= \nu e^{2\boldsymbol{a}\cdot\boldsymbol{V}_{\mathrm{d}}} j_z^{\mathrm{ro}\pm},
\end{aligned}
$$

the Vlasov-Maxwell equations become (for $\alpha_+ = 0$)

$$a_y'' + \beta^\infty[\frac{V_{\mathrm{ry}}}{2} Q(\boldsymbol{a}) + V_{\mathrm{dy}}\bar{Q}(\boldsymbol{a})] = 0, \quad \text{(A1)}$$

$$a_z'' + \beta^\infty[\frac{V_{\mathrm{rz}}}{2} Q(\boldsymbol{a}) + \hat{Q}(\boldsymbol{a})] = 0, \quad \text{(A2)}$$

with

$$
\begin{aligned}
Q(\boldsymbol{a}) &= \frac{1}{2}(1+\nu e^{2\boldsymbol{a}\cdot\boldsymbol{V}_{\mathrm{d}}})\sinh(\boldsymbol{a}\cdot\boldsymbol{V}_{\mathrm{r}})\cdot\\
&\qquad [e^{-\phi} g_{\lambda_+} + e^{\phi}(\hat{g}_{\lambda_-} + \alpha_- g_{\lambda_-})],\\
\bar{Q}(\boldsymbol{a}) &= \frac{1}{2}\nu e^{2\boldsymbol{a}\cdot\boldsymbol{V}_{\mathrm{d}}}\cosh(\boldsymbol{a}\cdot\boldsymbol{V}_{\mathrm{r}})\cdot\\
&\qquad [e^{-\phi} f_{\lambda_+} + e^{\phi}(\hat{f}_{\lambda_-} + \alpha_- f_{\lambda_-})],\\
\hat{Q}(\boldsymbol{a}) &= \frac{1}{2\sqrt{\pi}}(1+\nu e^{2\boldsymbol{a}\cdot\boldsymbol{V}_{\mathrm{d}}})\sinh(\boldsymbol{a}\cdot\boldsymbol{V}_{\mathrm{r}})\cdot\\
&\qquad [\lambda_-(1-\alpha_-) e^{\phi-\lambda_-^2 a_z^2} - \lambda_+ e^{-\phi-\lambda_+^2 a_z^2}].
\end{aligned}
$$

An approximation for $|x| < \min\{\mathcal{L}_{\mathrm{d}}, \mathcal{L}_+, \mathcal{L}_-\}$ can be derived (assuming $\theta^0 = 0°$):

$$
\begin{aligned}
a_y(x) &\approx 0, \qquad a_z(x) \approx -B_y^0 x,\\
f_\lambda(x) &\approx 1 - \frac{2\lambda}{\sqrt{\pi}} V_{\mathrm{rz}} a_z^2, \qquad g_\lambda(x) \approx 1 - \frac{2\lambda}{\sqrt{\pi V_{\mathrm{rz}}}},\\
\hat{f}_\lambda(x) &\approx 1 + \frac{2\lambda}{\sqrt{\pi}} V_{\mathrm{rz}} a_z^2, \qquad \hat{g}_\lambda(x) \approx 1 + \frac{2\lambda}{\sqrt{\pi V_{\mathrm{rz}}}}.
\end{aligned}
$$

Maxwell's equations (A1) and (A2) are simplified to

$$a_y'' + \nu\beta^\infty\sqrt{1+\alpha_-} V_{\mathrm{dy}} \approx 0, \quad \text{(A3)}$$

$$a_z'' + \frac{\beta^\infty}{2}(1+\nu)\sqrt{1+\alpha_-} V_{\mathrm{rz}}(V_{\mathrm{rz}} + \hat{V}_{\mathrm{r}}) a_z \approx 0, \quad \text{(A4)}$$

with $\hat{V}_{\mathrm{r}}$ as defined in equation (10). The corresponding magnetic field profile is

$$B_z \approx -\nu\beta^\infty\sqrt{1+\alpha_-} V_{\mathrm{dy}} x, \quad \text{(A5)}$$

$$B_y \approx B_y^0[1 - \frac{\beta^\infty}{4}(1+\nu)\sqrt{1+\alpha_-} V_{\mathrm{rz}}(V_{\mathrm{rz}} + \hat{V}_{\mathrm{r}}) x^2]. \quad \text{(A6)}$$

Equation (A5) shows how B_z linearly reverses its sign at the center of the transition; the sign of B_z' is opposite to that of V_{dy}. From (A5) and (A6) one can conclude that the magnetic field hodogram has a parabolic shape at the center.

In the absence of inner populations, Maxwell's equations show that a_y'' and a_z'' are odd functions of $\boldsymbol{a}$ and that f, $\hat{f}$, g, and $\hat{g}$ are all even functions of $\boldsymbol{a}$. When $\theta^0 = 0°$ and $\boldsymbol{a}(0) = \boldsymbol{0}$, it follows that $a_y(x)$ and $a_z(x)$, and hence also $B_y(x)$ and $B_z(x)$, must be even: there is no net magnetic field rotation.

When $V_{\mathrm{ry}} = 0$ and V_{rz} is small, the drift current dominates the transition, and the Vlasov-Maxwell equations can be approximated up to moderate $|x|$ values by

$$a_y \approx -\frac{1}{V_{\mathrm{dy}}} \ln\cosh\frac{x}{\mathcal{L}'}, \quad \text{(A7)}$$

$$a_z'' - (1 + \frac{\nu}{\cosh^2\frac{x}{\mathcal{L}'}})\frac{\beta^\infty}{2}\sqrt{1+\alpha_-} V_{\mathrm{rz}}(V_{\mathrm{rz}} + \hat{V}_{\mathrm{r}}) a_z \approx 0, \quad \text{(A8)}$$

where $\mathcal{L}' = 1/\sqrt{\nu\beta^\infty\sqrt{1+\alpha_-} V_{\mathrm{d}}}$ is the transition length scale. Abandoning the dimensionless notation, one finds

$$\mathcal{L}' = \frac{\rho^+ V_{\mathrm{th}}^+}{\sqrt{\nu\beta^\infty\sqrt{1+\alpha_-} V_{\mathrm{d}}}}.$$

For $\alpha_\pm = 0$ and $\boldsymbol{V}_{\mathrm{r}} = \boldsymbol{0}$ one obtains the modified Harris transition (used by *Galeev et al.* [1986]); noting that $\nu\beta^\infty = 4\mu_0 N^{\mathrm{i}} kT^\infty / B^{\infty 2}$ and computing $N^{\mathrm{i}} = B_z^{\infty 2}/4\mu_0 kT^\infty$ from the pressure balance, we find the transition length to be:

$$\mathcal{L}' = \frac{\rho^+ V_{\mathrm{th}}^+ B^\infty}{V_{\mathrm{d}} B_z^\infty} = \frac{2kT^\infty}{eV_{\mathrm{d}} B_z^\infty} = \frac{\mathcal{L}_{\mathrm{d}}}{\sin(\theta/2)}. \quad \text{(A9)}$$

For a field reversal ($\theta = 180°$) the transition length is $\mathcal{L}' = \mathcal{L}_{\mathrm{d}} = \mathcal{L}_{\mathrm{H}}$, the scale length derived in the Harris model [*Harris*, 1962].

Appendix B: Sufficient Condition

This appendix presents a more rigorous derivation of the sufficient conditions (11) and (12). When $V_{\mathrm{ry}} = 0$, the Vlasov-Maxwell equations are simplified to

$$a_y'' + \beta^\infty V_{\mathrm{dy}}\bar{Q}(\boldsymbol{a}) = 0, \quad \text{(B1)}$$

$$a_z'' - \frac{\beta^\infty}{4}(1+\nu e^{2a_y V_{\mathrm{dy}}})\sinh(a_z V_{\mathrm{rz}}) A(a_z) = 0, \quad \text{(B2)}$$

where $A(a_z)$ is given by

$$
\begin{aligned}
A(a_z) &= \frac{2}{\sqrt{\pi}}[\lambda_+ e^{-\phi-\lambda_+^2 a_z^2} - \lambda_-(1-\alpha_-) e^{\phi-\lambda_-^2 a_z^2}]\\
&\quad - V_{\mathrm{rz}}[e^{-\phi} g_{\lambda_+} + e^{+\phi}(\hat{g}_{\lambda_-} + \alpha_- g_{\lambda_-})].
\end{aligned}
$$

When $\theta^0 = 0°$, $B_y(x)$ is even while $B_z(x)$ is odd: the magnetic field hodogram has mirror symmetry about the y axis (as in Figure 6b), and the (X, Y, Z) and (x, y, z) frames coincide. As the second term in (B1) always has the same sign,

B_z varies monotonously. Consider the particular situation in which $\mathcal{L}_+ > \mathcal{L}_-$, i.e. $\lambda_+ < \lambda_-$:

$$A(a_z) \approx \frac{2\lambda_+}{\sqrt{\pi}} e^{-\lambda_+^2 a_z^2}, \quad |a_z| \text{ large},$$

$$A(a_z) \approx -2\sqrt{1+\alpha_-}(V_{rz} + \hat{V}_r), \quad |a_z| \text{ small},$$

with $\hat{V}_r$ as defined in equation (10). The $a_z(x)$ profile is found by integrating equation (B2) starting from $a_z(0) = 0$. Given $\theta^0 = 0°$ (i.e., $B_y(0) > 0$), one has $\operatorname{sign} a_z'(x) = -\operatorname{sign} x$ close to the transition center. There are now three different possibilities: (1) if $V_{rz} > 0$, then $\operatorname{sign} a_z''(x) = +\operatorname{sign} x$, (2) if $-\hat{V}_r \le V_{rz} \le 0$, then $\operatorname{sign} a_z''(x) = -\operatorname{sign} x$, and (3) if $V_{rz} < -\hat{V}_r$, then $\operatorname{sign} a_z''(x) = +\operatorname{sign} x$. In cases (1) and (3) the a_z profile may oscillate. In case (2), B_y increases with x; whatever the precise behavior of $A(a_z)$ for intermediate values of a_z, it is known to decrease very fast for large $|a_z|$, and so one expects $B_y(x)$ to remain positive everywhere; a solution matching the boundary conditions can then be found. Similarly, for $\theta^0 = 180°$ ($B_y(0) < 0$) one finds that a solution with $B_y^\infty < 0$ usually exists for $0 \le V_{rz} \le \hat{V}_r$. The same reasoning applies to the situation $\mathcal{L}_+ < \mathcal{L}_-$, but with the sign of V_{rz} reversed. These are precisely the sufficient conditions (11) and (12) derived earlier.

Acknowledgments. The authors thank M. M. Kuznetsova, B. T. Tsurutani, and J. F. Lemaire for interesting discussions and valuable comments. M. R. is grateful to D. Hubert (Observatoire de Paris, Meudon, France) for his kind hospitality and stimulating discussions that were at the origin of this study. Part of the work described in this paper was performed at the Belgian Institute for Space Aeronomy under a PRODEX contract with ESA in the framework of the Ulysses Interdisciplinary Study on Directional Discontinuities. We acknowledge the support of the Belgian Federal Services for Scientific, Technical, and Cultural Affairs.

The Editor thanks Timothy E. Eastman and another referee for their assistance in evaluating this paper.

References

Behannon, K. W., F. M. Neubauer, and H. Barnstorf, Fine-scale characteristics of interplanetary sector boundaries, *J. Geophys. Res., 86*, 3273–3287, 1981.

Berchem, J., and C. T. Russell, The thickness of the magnetopause current layer: ISEE 1 and 2 observations, *J. Geophys. Res., 87*, 2108–2114, 1982a.

Berchem, J., and C. T. Russell, Magnetic field rotation through the magnetopause: ISEE 1 and 2 observations, *J. Geophys. Res., 87*, 8139–8148, 1982b.

Cargill, P. J., and T. E. Eastman, The structure of tangential discontinuities, 1, Results of hybrid simulations, *J. Geophys. Res., 96*, 13,763–13,779, 1991.

Davies, C. M., The boundary layer between a cold plasma and a confined magnetic field when the plasma is not normally incident on the boundary, *Planet. Space Sci., 16*, 1249-1257, 1968.

Davies, C. M., The structure of the magnetopause, *Planet. Space Sci., 17*, 333–338, 1969.

De Keyser, J., M. Roth, B. T. Tsurutani, C. M. Ho, and J. L. Phillips, Solar wind velocity jumps across tangential discontinuities: Ulysses observations and kinetic interpretation, *Astron. Astrophys.*, in press, 1997.

Eastman, T. E., E. W. Hones Jr., S. J. Bame, and J. R. Asbridge, The magnetospheric boundary layer: Site of plasma, momentum and energy transfer from the magnetosheath into the magnetosphere, *Geophys. Res. Lett., 3*, 685–688, 1976.

Eastman, T. E., S. A. Fuselier, and J. T. Gosling, Magnetopause crossings without a boundary layer, *J. Geophys. Res., 101*, 49–57, 1996.

Ferraro, V. C. A., and C. M. Davies, Discussion of paper by E. N. Parker, "Confinement of a magnetic field by a beam of ions," *J. Geophys. Res., 73*, 3605–3606, 1968.

Fuselier, S. A., E. G. Shelly, and D. M. Klumpar, Mass density and pressure changes across the dayside magnetopause, *J. Geophys. Res., 98*, 3935–3942, 1993.

Galeev, A. A., M. M. Kuznetsova, and L. M. Zelenyi, Magnetopause stability threshold for patchy reconnection, *Space Sci. Rev., 44*, 1, 1986.

Harris, E. G., On a plasma sheath separating regions of oppositely directed magnetic field, *Nuovo Cimento, 23*, 115–121, 1962.

Kuznetsova, M. M., and M. Roth, Thresholds for magnetic percolation through the magnetopause current layer in asymmetrical magnetic fields, *J. Geophys. Res., 100*, 155, 1995.

Kuznetsova, M. M., M. Roth, Z. Wang, and M. Ashour-Abdalla, Effect of the relative flow velocity on the structure and stability of the magnetopause current layer, *J. Geophys. Res., 99*, 4095–4104, 1994.

Le, G., and C. T. Russell, The thickness and structure of high beta magnetopause current layer, *Geophys. Res. Lett., 21*, 2451–2454, 1994.

Lee, L. C., and J. R. Kan, A unified kinetic model of the tangential magnetopause structure, *J. Geophys. Res., 84*, 6417–6426, 1979.

Lerche, I., On the boundary layer between a warm, streaming plasma and a confined magnetic field, *J. Geophys. Res., 72*, 5295–5310, 1967.

Lerche, I., and E. N. Parker, Non-equilibrium and enhanced mixing at a plasma-field interface, *Astrophys. J., 150*, 731–732, 1967.

Lerche, I., and E. N. Parker, Comments on "Steady state charge neutral models of the magnetopause," *Astrophys. Space Sci., 8*, 140, 1970.

Papamastorakis, I., G. Paschmann, and N. Sckopke, The magnetopause as a tangential discontinuity for large field rotation angles, *J. Geophys. Res., 89*, 127–135, 1984.

Parker, E. N.., Confinement of a magnetic field by a beam of ions, *J. Geophys. Res., 72*, 2315–2322, 1967a.

Parker, E. N.., Small-scale nonequilibrium of the magnetopause and its consequences, *J. Geophys. Res., 72*, 4365–4374, 1967b.

Parker, E. N., Dynamical properties of the magnetosphere, in *Physics of the Magnetosphere*, edited by R. L. Carovillano, J. F. McClay, and H. F. Radoski, p. 3, D. Reidel, Norwell, Mass., 1968.

Parker, E. N., Solar wind interaction with the geomagnetic field, *Rev. Geophys., 7*, 3–10, 1969.

Paschmann, G., I. Papamastorakis, W. Baumjohann, N. Sckopke, C. W. Carlson, B. U. Ö. Sonnerup, and H. Lühr, The magnetopause for large magnetic shear: Ampte/Irm observations, *J. Geophys. Res., 91*, 11,099–11,119, 1986.

Phan, T. D., and G. Paschmann, Low-latitude dayside magnetopause and boundary layer for high magnetic shear, 1, Structure and motion, *J. Geophys. Res., 101*, 7801–7815, 1996.

Roth, M., J. Lemaire, and A. Misson, An iterative method to solve the nonlinear Poisson's equation in the case of plasma tangential discontinuities, *J. Comput. Phys., 86*, 466, 1990.

Roth, M., J. De Keyser, and M. M. Kuznetsova, Vlasov theory of the equilibrium structure of tangential discontinuities in space plasmas, *Space Sci. Rev., 76*, 251–317, 1996.

Sestero, A., Vlasov equation study of plasma motion across magnetic fields, *Phys. Fluids, 9*, 2006–2013, 1966.

Sonnerup, B. U. Ö., and L. J. Cahill, Magnetopause structure and attitude from Explorer 12 observations, *J. Geophys. Res., 72*, 171–183, 1967.

Sonnerup, B. U. Ö., and L. J. Cahill, Explorer 12 observations of the magnetopause current layer, *J. Geophys. Res., 73,* 1757–1770, 1968.

Storey, L. R. O., and L. Cairo, Kinetic theory of the boundary layer between a flowing isotropic plasma and a magnetic field, in *Magnetospheric Boundary Layers*, edited by B. Battrick and J. Mort, p. 289, *ESA Spec. Publ., SP-148*, Eur. Space Agency, Neuilly, France, 1979.

Su, S.-Y., and B. U. Ö. Sonnerup, First-order orbit theory of the rotational discontinuity, *Phys. Fluids, 11*, 851–857, 1968.

Su, S.-Y., and B. U. Ö. Sonnerup, On the equilibrium of the magnetopause layer, *J. Geophys. Res., 76*, 5181–5188, 1971.

Whipple, E. C., J. R. Hill, and J. D. Nichols, Magnetopause structure and the question of accessibility, *J. Geophys. Res., 89,* 1508–1516, 1984.

Willis, D. M., The microstructure of the magnetopause, *Geophys. J. R. Astron. Soc., 41*, 355–389, 1975.

Wu, Z.-J., Solar wind particle trajectories in the magnetopause, *Ann. Geophys., Ser. A, 4*, 41–48, 1986a.

Wu, Z.-J., On microscopic stress nonequilibrium: Application to the magnetopause, *Ann. Geophys., Ser. A, 4*, 341–354, 1986b.

J. De Keyser and M. Roth, Belgian Institute for Space Aeronomy (BIRA/IASB), Ringlaan 3, B-1180 Brussels, Belgium. (e-mail: Johan.DeKeyser@oma.be; Michel.Roth@oma.be)

(Received July 31, 1996; revised December 27, 1996; accepted January 28, 1997.)